

# 1 Global Greenhouse Gas Reconciliation 2022

2 Zhu Deng<sup>1,2,3</sup>, Philippe Ciais<sup>4,\*</sup>, Liting Hu<sup>5</sup>, Adrien Martinez<sup>4</sup>, Marielle Saunois<sup>4</sup>, Rona L. Thompson<sup>6</sup>,  
3 Kushal Tibrewal<sup>4</sup>, Wouter Peters<sup>7,8</sup>, Brendan Byrne<sup>9</sup>, Giacomo Grassi<sup>10</sup>, Paul I. Palmer<sup>11,12</sup>, Ingrid T.  
4 Luijkx<sup>7</sup>, Zhu Liu<sup>1,2,3,\*</sup>, Junjie Liu<sup>9,13</sup>, Xuekun Fang<sup>5</sup>, Tengjiao Wang<sup>14</sup>, Hanqin Tian<sup>15</sup>, Katsumasa  
5 Tanaka<sup>4,16</sup>, Ana Bastos<sup>17</sup>, Stephen Sitch<sup>18</sup>, Benjamin Poulter<sup>19</sup>, Clément Albergel<sup>20</sup>, Aki Tsuruta<sup>21</sup>, Shamil  
6 Maksyutov<sup>16</sup>, Rajesh Janardanan<sup>16</sup>, Yosuke Niwa<sup>16,22</sup>, Bo Zheng<sup>23,24</sup>, Joël Thanwerdas<sup>25</sup>, Dmitry  
7 Belikov<sup>26</sup>, Arjo Segers<sup>27</sup>, Frédéric Chevallier<sup>4</sup>

8 <sup>1</sup>Department of Geography, University of Hong Kong, Hong Kong SAR, China

9 <sup>2</sup>Institute for Climate and Carbon Neutrality, University of Hong Kong, Hong Kong SAR, China

10 <sup>3</sup>Department of Earth System Science, Tsinghua University, Beijing, China

11 <sup>4</sup>Laboratoire des Sciences du Climat et de l'Environnement, IPSL, CEA-CNRS-UVSQ, Université Paris-Saclay, Gif-sur-  
12 Yvette, France

13 <sup>5</sup>College of Environmental & Resource Sciences, Zhejiang University, Hangzhou, Zhejiang, China

14 <sup>6</sup>Norwegian Institute for Air Research (NILU), Kjeller, Norway

15 <sup>7</sup>Meteorology and Air Quality Department, Wageningen University & Research, Wageningen, the Netherlands

16 <sup>8</sup>Energy and Sustainability Research Institute Groningen, University of Groningen, Groningen, the Netherlands

17 <sup>9</sup>Jet Propulsion Laboratory, California Institute of Technology, Pasadena, CA, USA

18 <sup>10</sup>Joint Research Centre, European Commission, Ispra (VA), Italy

19 <sup>11</sup>National Centre for Earth Observation, University of Edinburgh, Edinburgh, UK

20 <sup>12</sup>School of GeoSciences, University of Edinburgh, Edinburgh, UK

21 <sup>13</sup>Division of Geological and Planetary Sciences, California Institute of Technology, Pasadena, CA, USA

22 <sup>14</sup>Institute of Blue and Green Development, Shandong University, Weihai, China

23 <sup>15</sup>International Center for Climate and Global Change Research, School of Forestry and Wildlife Sciences, Auburn University,  
24 Auburn, AL 36849, USA

25 <sup>16</sup>Earth System Division, National Institute for Environmental Studies, Onogawa 16-2, Tsukuba, Ibaraki 305-8506, Japan

26 <sup>17</sup>Institute for Earth System Science and Remote Sensing, Leipzig University, 04103 Germany

27 <sup>18</sup>Faculty of Environment, Science and Economy, University of Exeter, Exeter, UK

28 <sup>19</sup>NASA Goddard Space Flight Center, Biospheric Sciences Laboratory, Greenbelt, MD 20771, USA

29 <sup>20</sup>European Space Agency Climate Office, ECSAT, Harwell Campus, Didcot, Oxfordshire, UK

30 <sup>21</sup>Finnish Meteorological Institute, P.O. Box 503, 00101, Helsinki, Finland

31 <sup>22</sup>Department of Climate and Geochemistry Research, Meteorological Research Institute (MRI), Nagamine 1-1, Tsukuba,  
32 Ibaraki 305-0052, Japan

33 <sup>23</sup>Shenzhen Key Laboratory of Ecological Remediation and Carbon Sequestration, Institute of Environment and Ecology,  
34 Tsinghua Shenzhen International Graduate School, Tsinghua University, Shenzhen, 518055, China

35 <sup>24</sup>State Environmental Protection Key Laboratory of Sources and Control of Air Pollution Complex, Beijing 100084, China

36 <sup>25</sup>Empa, Swiss Federal Laboratories for Materials Science and Technology, Dübendorf, Switzerland

37 <sup>26</sup>Center for Environmental Remote Sensing, Chiba University, Chiba, Japan

38 <sup>27</sup>TNO, Department of Air quality and Emissions Research, P.O. Box 80015, NL-3508-TA, Utrecht, the Netherland

39 *Correspondence to:* Philippe Ciais ([philippe.ciais@lsce.ipsl.fr](mailto:philippe.ciais@lsce.ipsl.fr)); Zhu Liu ([zhuliu@tsinghua.edu.cn](mailto:zhuliu@tsinghua.edu.cn))

删除了: [hku.hk](mailto:hku.hk)

40 **Abstract.** In this study, we provide an update of the methodology and data used by Deng et al. (2022) to compare the national  
41 greenhouse gas inventories (NGHGs) and atmospheric inversion model ensembles contributed by international research teams

43 coordinated by the Global Carbon Project. The comparison framework uses transparent processing of the net ecosystem  
44 exchange fluxes of carbon dioxide (CO<sub>2</sub>) from inversions to provide estimates of terrestrial carbon stock changes over managed  
45 land that can be used to evaluate NGHGs. For methane (CH<sub>4</sub>), and nitrous oxide (N<sub>2</sub>O), we separate anthropogenic emissions  
46 from natural sources based directly on the inversion results, to make them compatible with NGHGs. Our global harmonized  
47 NGHGs database was updated with inventory data until February 2023 by compiling data from periodical UNFCCC  
48 inventories by Annex I countries and sporadic and less detailed emissions reports by non-Annex I countries given by National  
49 Communications and Biennial Update Reports. For the inversion data, we used an ensemble of 22 global inversions produced  
50 for the most recent assessments of the global budgets of CO<sub>2</sub>, CH<sub>4</sub> and N<sub>2</sub>O coordinated by the Global Carbon Project with  
51 ancillary data. The CO<sub>2</sub> inversion ensemble in this study goes through 2021, building on our previous report from 1990 to  
52 2019, and includes three new satellite inversions compared to the previous study, and an improved managed land mask. As a  
53 result, although significant differences exist between the CO<sub>2</sub> inversion estimates, both satellite and in-situ inversions over  
54 managed lands indicate that Russia and Canada had a larger land carbon sink in recent years than reported in their NGHGs,  
55 while the NGHGs reported a significant upward trend of carbon sink in Russia but a downward trend in Canada. For CH<sub>4</sub> and  
56 N<sub>2</sub>O, the results of the new inversion ensembles are extended to 2020. Rapid increases in anthropogenic CH<sub>4</sub> emissions were  
57 observed in developing countries, with varying levels of agreement between NGHGs and inversion results, while developed  
58 countries showed a slow declining or stable trend in emissions. Much denser sampling of atmospheric CO<sub>2</sub> and CH<sub>4</sub>  
59 concentrations by different satellites, coordinated into a global constellation, is expected in the coming years. The methodology  
60 proposed here to compare inversion results with NGHGs can be applied regularly for monitoring the effectiveness of  
61 mitigation policy and progress by countries to meet the objective of their pledges. The dataset constructed for this study is  
62 publicly available at <https://doi.org/10.5281/zenodo.13887128> (Deng et al., 2024).

## 63 **1 Introduction**

64 If modeled pathways align with Nationally Determined Contributions (NDCs) declared prior to COP26 (in 2021) until 2030  
65 and do not involve any subsequent increase in ambition, the projected global warming by 2100 would be 2.1-3.4°C (IPCC,  
66 2023). The global stocktake coordinated by the secretariat of the United Nations Framework Convention on Climate Change  
67 (UNFCCC) considers data from national greenhouse gas inventories (NGHGs) to assess the collective climate progress to  
68 curb emissions. It is expected there will be differences in the quality of NGHGs being reported to the UNFCCC (Perugini et  
69 al., 2021). UNFCCC Annex I Parties, which include all OECD (Organisation for Economic Co-operation and Development)  
70 countries and several EIT (Economies In Transition) already report annually their emissions following the same IPCC  
71 guidelines (IPCC 2006) in a common reporting format, with a time latency of roughly 1.5 years. In contrast, non-Annex I  
72 Parties, mostly developing and less developed countries, are currently not required to provide reports as regularly and as  
73 detailed as Annex I Parties and in a few cases use different IPCC Guidelines in their National Communications (NC) or  
74 Biennial Update Reports (BUR) submitted to the UNFCCC. Non-Annex I Parties are scheduled in 2024 to move to regular

75 and harmonized reporting of their emissions in the national inventory reports (NIRs) in the format of common reporting tables  
76 (CRTs), following the Paris Agreement's enhanced transparency framework (ETF).

77 The IPCC guidelines for NGHGs encourage countries to use independent information to verify emissions and removals (IPCC,  
78 1997, 2006, 2019), such as comparisons with independently compiled inventory databases (e.g. IEA, CDIAC, EDGAR,  
79 FAOSTAT), or with atmospheric mole fraction measurements interpreted by atmospheric inversion models (see Section 6.10.2  
80 in IPCC (2019)). Such verification of 'bottom-up' national reports against 'top-down' atmospheric inversion results is not  
81 mandatory. However, a few countries (e.g. Switzerland, United Kingdom, New Zealand, and Australia) have already added  
82 inversions as a consistency check of their national reports. In our study, we utilized the latest global inversion results from the  
83 budget assessments of CO<sub>2</sub>, CH<sub>4</sub>, and N<sub>2</sub>O conducted by the Global Carbon Project (GCP), focusing on three ensembles of  
84 inversions with global coverage. Compared to our previous study (Deng et al., 2022), the CO<sub>2</sub> inversion ensemble used in this  
85 study has been updated to the global CO<sub>2</sub> budget of Friedlingstein et al. (2022) that includes nine CO<sub>2</sub> inversions using mole  
86 fraction data from the surface network and/or retrieval products from the Greenhouse Gases Observing Satellite (GOSAT) and  
87 Orbiting Carbon Observatory-2 (OCO-2) satellites. The CH<sub>4</sub> inversion ensemble and N<sub>2</sub>O inversion (Tian et al., 2023)  
88 ensemble used in this study are also extended to the 2020. As a result, the new ensembles cover up to 2021 for CO<sub>2</sub>, 2020 for  
89 CH<sub>4</sub> and 2020 for N<sub>2</sub>O, compared to 2019, 2017 and 2016 respectively in our previous study (Deng et al., 2022), allowing us  
90 to track and analyze the most recent flux variations.

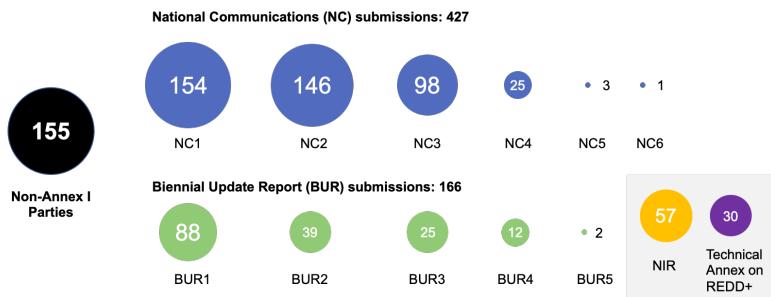
91 Our framework to process the inversion data aims at making them comparable to inventories at countries or groups of countries  
92 scale (ie, with an area larger than the spatial resolution of atmospheric transport models typically used for inversions).  
93 Atmospheric inversions use *a priori* information for the spatial and temporal patterns of fluxes. Some inversions correct prior  
94 fluxes at the spatial resolution of their transport models to match atmospheric observations and use spatial error correlations  
95 (usually e-folding length scales) that tie the adjustment of fluxes from one grid cell to its neighbors at distances of tens to  
96 hundreds of kilometers. Other inversions adjust fluxes over coarse regions that are larger than the resolution of the transport  
97 model, implicitly assuming a perfect correlation of flux errors within these regions, causing an aggregation error (Kaminski et  
98 al., 2001). Thus, to minimize aggregation errors, the results of inversions are shown preferentially for selected large area  
99 emitter countries or large absorbers in the case of CO<sub>2</sub>. We have selected a different set of countries or groups of countries for  
00 each gas, according to their importance in the global emission budget. According to the median of inversion data we used in  
01 this study, selected countries collectively represent ~70% of global fossil fuel CO<sub>2</sub> emissions, ~90% of global land CO<sub>2</sub> sink, ~  
02 60% of anthropogenic CH<sub>4</sub> emissions, and ~55% of anthropogenic N<sub>2</sub>O emissions (Fig S1). To more robustly interpret global  
03 inversion results for comparison with inventories, we follow the same criterion and choose high-emitting countries covered (if  
04 possible) by atmospheric measurements, although most selected tropical countries have few or no atmospheric in-situ stations.  
05 Uncertainties are given by the spread among inversion models (min-max range given the small number of inversions), and the  
06 causes for discrepancies with inventories are analyzed systematically and on a case-by-case basis, considering both individual  
07 countries and specific greenhouse gases, for annual variations and for mean budgets over several years.

08 Based on the newly updated inversion results and inventory, and an improvement in the methodology framework proposed in  
 09 the previous study (Deng et al., 2022), we specifically address the following questions: 1) how do inversion models compare  
 10 with NGHGs for the three gases?; 2) what are the plausible reasons for mismatches between inversions and NGHGs?; 3) did  
 11 the new maps of managed land masks in this study reduce the mismatch between the inversions and NGHGs for CO<sub>2</sub> and  
 12 N<sub>2</sub>O?; 4) what independent information can be extracted from inversions to evaluate the mean values or the trends of  
 13 greenhouse gas emissions and removals?; 5) does this information exhibit a good agreement with NGHGs?; and 6) how do  
 14 satellite-retrieval driven inversion models differ from the surface in-situ and flask sampling driven inversion model results?  
 15 Sections 2 presents the updated global database of national emissions reports for selected countries and its grouping into sectors,  
 16 the global atmospheric inversions used for the study, the processing of fluxes from these inversions to make their results as  
 17 comparable as possible with inventories. The time series of inversions compared with inventories for each gas, with insights  
 18 on key sectors for CH<sub>4</sub> are discussed in **Sections 3 to 5**. The discussion (Section 6) focuses on the plausible reasons for  
 19 mismatches between inversions and NGHGs, comparison between inversion ensembles in this study and previous study, and  
 20 different priors applied in the CH<sub>4</sub> inversions. Finally, concluding remarks are drawn on how inversions could be used  
 21 systematically to support the evaluation and possible improvement of inventories for the Paris Agreement.

## 22 2 Material and methods

### 23 2.1 Compilation and harmonization of national inventories reported to the UNFCCC

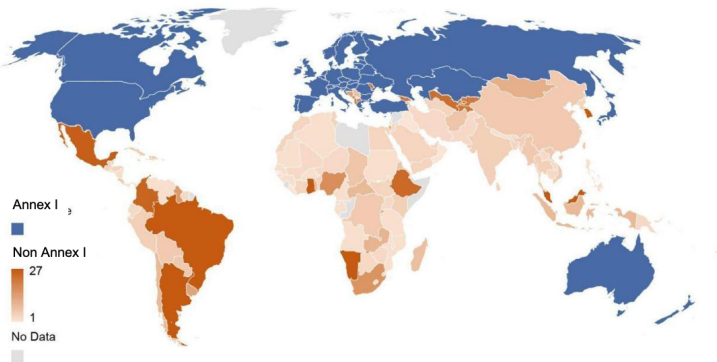
24 All UNFCCC Parties shall periodically update and submit their national GHG inventories of emissions by sources and  
 25 removals by sinks to the Convention parties. Annex I countries submit their NIRs in common reporting format (CRF) tables  
 26 every year with a complete time series starting in 1990. Non-Annex I Parties are required to submit their NC roughly every  
 27 four years after entering the Convention and submit BUR, every two years since 2014. Currently, there are in total 427  
 28 submissions of NC and over 166 submissions of BUR (UNFCCC, 2021b, a) (**Fig 1**).



29

30 **Figure 1. Numbers of non-Annex I parties for each submission round (as of February 28, 2023).** The numbers in the middle of the dots  
31 denote the numbers of non-Annex I parties for each submission, while the black dots denote the total number of non-Annex I parties, the  
32 blue dots denote the numbers of non-Annex I parties who has submitted National Communications (NC), green dots for Biennial Update  
33 Reports (BUR), yellow dots for National Inventory Report (NIR), and purple dots for Technical Annex on REDD+ . The numbers after the  
34 NC and BUR denote the total number of submission reports.

35 We collected NGHGs data submitted to UNFCCC by February 28, 2023. For Annex I countries, data collection is  
36 straightforward, as their reports are provided as Excel files under a Common Reporting Format (CRF) until the year 2020 last  
37 accessed on February 28, 2023. For non-Annex I countries, the data were directly extracted from the original reports provided  
38 in Portable Document Format (PDF) last accessed on February 28, 2023. Data from successive reports for the same country  
39 were extracted, except when they relate to the same years, in which case only the latest version is considered. While Annex I  
40 countries are required to compile their inventory following IPCC 2006 guidelines and the subdivision between sectors  
41 established by the UNFCCC decision (dec. 24/CP.19), non-Annex I countries are increasingly adopting the IPCC 2006  
42 Guidelines, although some still utilize the older IPCC 1996 Guidelines, with different approaches and sectors. Consequently,  
43 the methods used and the reported sectors may differ among NC and BUR reports.



44 **Figure 2. Number of years covered by NGHGI reports (NC+BUR) in each non-Annex I country (as of February 28, 2023).** Emissions  
45 from Greenland are reported by Denmark.  
46

## 47 2.2 Atmospheric inversions

### 48 CO<sub>2</sub> inversions

49 Nine CO<sub>2</sub> inversion systems from the 2022 Global Carbon Budget of the GCP (Friedlingstein et al., 2022) are used, including  
50 CarbonTracker-Europe (CTE) v2022 (van der Laan-Luijkx et al., 2017), Jena Carboscope v2022 (Rödenbeck et al., 2003), the

51 surface air-sample inversion from the Copernicus Atmosphere Monitoring Service (CAMS) v21r1 (Chevallier et al., 2005),  
 52 the inversion from the CAMS Satellite FT21r2 (Chevallier et al., 2005), the inversion from the University of Edinburgh (UoE)  
 53 v6.1b (Feng et al., 2016), the NICAM-based Inverse Simulation for Monitoring CO<sub>2</sub> (NISMON-CO<sub>2</sub>) v2022.1 (Niwa et al.,  
 54 2022), CMS-Flux v2022 (Liu et al., 2021), GONGGA v2022 (Jin et al., 2023), and THU v2022 (Kong et al., 2022). A variety  
 55 of transport models are used by these systems, which allows for representing a major driver factor behind differences in flux  
 56 estimates based on atmospheric inversions, particularly their distribution over latitudinal bands. Among the nine inversions,  
 57 four systems (CAMS Satellite FT21r2, GONGGA v2022, THU v2022, and CMS-Flux v2022) utilize satellite CO<sub>2</sub> column  
 58 retrievals from GOSAT and/or OCO-2, calibrated to the World Meteorological Organization (WMO) 2019 standards. CMS-  
 59 Flux additionally incorporates in-situ observed CO<sub>2</sub> mole fraction records. The remaining five inversion systems (CAMS v21r1,  
 60 CTE v2022, Jena Carboscope v2022, UoE v6.1b, and NISMON-CO<sub>2</sub> v2022.1) solely rely on CO<sub>2</sub> mole fractions that were  
 61 observed in-situ or collected in flasks (Schuldt et al., 2021, 2022). The CO<sub>2</sub> inversion records extend up to and including 2021.  
 62 Their flux estimates are available at [https://meta.icos-cp.eu/objects/GahdRITjT22GGmq\\_GCi4o\\_wy](https://meta.icos-cp.eu/objects/GahdRITjT22GGmq_GCi4o_wy) and details are  
 63 summarized in **Table 1**.

64 **Table 1 | Atmospheric CO<sub>2</sub> inversions used in this study** (Friedlingstein et al., 2022)

Inversion System	Version	Period	Observation	Transport Model
CarbonTracker Europe (CTE): CTE2022_SiB4 (van der Laan-Luijkx et al., 2017)	v2022	2001-2021	Ground-based  Obspack GLOBALVIEW plus v7.0 and NRT_v7.2	TM5
Jena Carboscope sEXTocNEET (Rödenbeck et al., 2003)	v2022	1960-2021		TM3
Copernicus Atmosphere Monitoring Service (CAMS) (Chevallier et al., 2005)	v21r1	1979-2021		LMDZ v6
The University of Edinburgh (UoE) (Feng et al., 2016)	v6.1b	2001-2021		GEOS-CHEM
the NICAM-based Inverse Simulation for Monitoring CO <sub>2</sub> (NISMON-CO <sub>2</sub> ) (Niwa et al., 2022)	v2022.1	1990-2021		NICAN-TM

CMS-Flux (Liu et al., 2021),	v2022	2010-2021	Ground-based & ACOS-GOSAT v9r; OCO-2 v10 scaled to WMO2019	GEOS-CHEM
CAMS-Satellite (Chevallier et al., 2005)	FT21r2	2010-2021	bias-corrected ACOS GOSAT v9 over land until August 2014 + bias- corrected ACOS OCO-2 v10 over land, both rescaled to WMO2019	LMDZ v6
THU (Kong et al., 2022)	v2022	2015-2021	OCO-2 v10r data scaled to WMO2019	GEOS-CHEM
GONGGA (Jin et al., 2023)	v2022	2015-2021	OCO-2 v10r data scaled to WMO2019	GEOS-CHEM

#### 65 CH<sub>4</sub> inversions

66 The CH<sub>4</sub> emissions come from the new ensemble of inversions (Saunois et al. 2024) from 2000 to 2020, using seven different  
67 inverse systems for a total nine inversions (**Table 2**). The inverse systems include: CarbonTracker-Europe CH<sub>4</sub> (Tsuruta et al.,  
68 2017), LMDZ-PYVAR (Yin et al., 2015; Zheng et al., 2018), CIF-LMDZ (Berchet et al., 2021), MIROC4-ACTM (Patra et al.,  
69 2018; Chandra et al., 2021), NISMON-CH<sub>4</sub> (Niwa et al., 2022), NIES-TM-FLEXPART (Maksyutov et al., 2021; Janardanan  
70 et al., 2024), and TM5-CAMS (Segers and Houweling, 2017). This ensemble of inversions gathers various chemistry transport  
71 models, differing in vertical and horizontal resolutions, meteorological forcing, advection (horizontal transport of air) and  
72 convection (vertical transport) schemes, and boundary layer mixing (detailed characteristics can be found in Table S11 in  
73 Saunois et al. 2024). Including these different systems is a conservative approach that allows to cover different potential  
74 uncertainties of the inversion, among them: model transport, set-up issues, and prior dependency. All inversions except two,  
75 use updated common prior emission maps for natural and anthropogenic prior emissions divided into 12 sectors, particularly  
76 the EDGAR v6 inventory for prior fossil fuel emissions (Crippa et al., 2021a extrapolated to Jan 1st, 2021), GFED for fires  
77 and ecosystem models for wetland emissions. During the production of the inversion simulations, GAINS inventory (Höglund-  
78 Isaksson, 2013) was proposed to use another prior for fossil fuel sources, ) instead of using EDGAR v6 (see Supplementary  
79 Text 3 in Saunois et al, 2024). GAINS has higher fossil emissions, in particular over the US and a higher increase of fossil  
80 emissions over time in the US (Tibrewal et al., 2024). As Tibrewal et al. showed that inversions are strongly attracted to their  
81 priors, comparison between results with GAINS and EDGAR v6 priors is informative about how robust are inversions to their  
82 priors when they are used to ‘verify’ NGHGs. Some inversions optimize emissions in groups of sectors, and others only  
83 provide total gridded emissions (MIROC4-ACTM and TM5-CAMS, details can be found in Table S10 in Saunois et al, 2024).  
84 For the latter, we computed the emission from each sector within each pixel based on the proportion of the prior fluxes. Such

85 processing can lead to significant uncertainties if not all sources increase or change at the same rate in a given region/pixel.  
 86 The inversions assimilating surface stations mole fraction observations provide results since 2000, and those assimilating  
 87 satellite observations from column CH<sub>4</sub> measurements (XCH<sub>4</sub>) of the GOSAT satellite provide results since 2010, first full  
 88 year of GOSAT observations. Inversion results were gridded into 1° by 1° monthly emission maps and aggregated nationally  
 89 using a country mask (Klein Goldewijk et al., 2017).

90 **Table 2 | Atmospheric CH<sub>4</sub> inversions used in this study (Saunois et al, 2024)**

Inversion system	Abbreviation	Institution	Observations	Period
Carbon Tracker-Europe CH4	CTE	FMI	Surface stations	2000-2020
CIF-LMDz	CIF-LMDz	LSCE/CEA	Surface stations	2000-2020
LMDz-PYVAR	PYVAR-LMDz	LSCE/CEA	GOSAT Leicester v7.2	2010-2020
MIROC4-ACTM	MIROC4-ACTM	JAMSTEC	Surface stations	2000-2020
NISMON-CH4	NISMON-CH4	NIES/MRI	Surface stations	2000-2020
NIES-TM-FLEXPART (NTF)	NIES	NIES	Surface stations	2000-2020
NIES-TM-FLEXPART (NTF)	NIES	NIES	Surface + GOSAT NIES L2 v02.95	2010-2020
TM5-CAMS	TM5	TNO/VU	Surface stations	2000-2020
TM5-CAMS	TM5	TNO/VU	GOSAT ESA/CCI v2.3.8 (combined with surface observations)	2010-2020



91 **N<sub>2</sub>O inversions**

92 Four N<sub>2</sub>O inversion systems from the updated GCP Nitrous Oxide Budget (Tian et al., 2023) are used: INVICAT (Wilson et  
93 al., 2014), PyVAR-CAMS (Thompson et al., 2014), MIROC4-ACTM (Patra et al., 2018, 2022) and GEOS-Chem (Wells et  
94 al., 2015). The N<sub>2</sub>O inversion results are updated up to 2020.

95 **Table 3 | Atmospheric N<sub>2</sub>O inversions used in this study** (Tian et al., 2023)

Inversion system	Institution	Period
INVICAT (Wilson et al., 2014)	Univ. Leeds	1995-2020
PyVAR-CAMS (Thompson et al., 2014),	NILU/LSCE	1995-2020
MIROC4-ACTM (Patra et al., 2018, 2022)	JAMSTEC	1997-2019
GEOS-Chem (Wells et al., 2015)	Univ. Minnesota	1995-2019

96 **Aggregating the gridded inversion results into national totals**

97 To obtain national annual-scale flux estimates, we aggregated the gridded flux maps of each inversion with various native  
98 resolutions following the methodology outlined in Chevallier (2021). This involved using the 0.08° x 0.08° land country mask  
99 of Klein Goldewijk et al. (2017) to calculate the fraction of each country in each inversion grid box.

:00 **2.3 Processing of CO<sub>2</sub> inversion data for comparison with NGHGs**

:01 **Fossil fuel emissions re-gridding - managed land mask**

:02 To analyze terrestrial CO<sub>2</sub> fluxes, we subtracted the same fossil fuel emissions (including cement) of GridFEDv2022.2 (Jones  
:03 et al., 2022) from the total CO<sub>2</sub> flux of each inversion. This is equivalent to assuming perfect knowledge of fossil emissions,  
:04 adding up to a global total of 9.7 GtC/yr for the year 2021. The dataset used national annual emissions estimates from the 2022  
:05 global carbon budget (Friedlingstein et al., 2022) which uses the reported NGHGs data from Annex I countries and are  
:06 assumed to be broadly consistent with the non-Annex I countries. This assumption may lead to underestimating the uncertainty  
:07 of terrestrial CO<sub>2</sub> fluxes deduced from inversions.

As defined in the IPCC Guidelines for NGHGs (IPCC, 2006), only CO<sub>2</sub> emissions and removals from managed land are reported in NGHGs as a proxy for human-induced effects (direct effects and indirect effects such as CO<sub>2</sub> fertilization and nitrogen deposition). However, inversion models retrieve all CO<sub>2</sub> fluxes (due to both direct and indirect effects, plus the natural interannual variability) over all lands. We thus retained inversions' national estimates of the Net Ecosystem Exchange (NEE) CO<sub>2</sub> flux ( $F_{ML}^{inv NEE}$ ) over managed lands grid cells only (*ML*, here defined as all land except intact forests) because the fluxes over unmanaged land are not counted by NGHGs. We use NEE from the definition of Ciais et al. (2020), representing all non-fossil CO<sub>2</sub> exchange fluxes between terrestrial surfaces and the atmosphere. Other work may use Net Biome Production (NBP) with a similar meaning. CO<sub>2</sub> fluxes over unmanaged lands were excluded from the terrestrial CO<sub>2</sub> flux totals that will be compared with NGHGs, proportional to their presence in each inversion grid box. The new maps of non-intact forests are compiled by Grassi et al. (2023). These maps include official country-managed forest and other managed land areas for Canada and Brazil used for their NGHGs, and the intact forest map (Potapov et al., 2017) as a substitute for unmanaged land where country-based information is not available. For Russia, we used non-intact forest maps for each province with thresholds adjusted to match the official managed land areas from Russia's NIRs, and assumed that all grasslands were managed. This approach assumes that non-intact forest areas can serve as a reasonably good proxy for managed forests reported in the NGHGs (Grassi et al., 2021, 2023). It is important to note that this approach is somewhat arbitrary, as highlighted in previous studies (Ogle et al., 2018; Chevallier, 2021; Grassi et al., 2021). However, in the absence of a machine-readable definition of managed plots in many NGHGs, there is currently no better alternative available.

#### Adjusting CO<sub>2</sub> fluxes due to lateral carbon transport by crop and wood products trade and by rivers

In addition to the extraction of fossil CO<sub>2</sub> flux and managed land CO<sub>2</sub> flux, there are CO<sub>2</sub> fluxes that are part of  $F_{ML}^{inv NEE}$  but are not counted by NGHGs. These fluxes are induced by (i) soils to rivers to oceans carbon export ( $F_{ML}^{rivers}$ ) which has an anthropogenic and a natural component (Regnier et al., 2013), and (ii) net anthropogenic export of crop and wood products across each country's boundary ( $F_{ant}^{crop trade}$  and  $F_{ant}^{wood trade}$ ). The magnitudes of these CO<sub>2</sub> fluxes are different between countries, and values from the selected countries are presented in **Fig S2**. We assume that NGHGs include CO<sub>2</sub> losses from fire (wildfire and prescribed fire) and other disturbances (wind, pests) and from domestic harvesting, as recommended by the IPCC reporting guidelines (IPCC, 2006, 2019) (although some countries, such as Canada and Australia exclude some emissions from these disturbances, and the subsequent removals from the same areas (Grassi et al., 2023)). The adjusted inversion NEE that can be compared with inventories,  $F_{adj}^{inv NEE}$ , is given by:

$$F_{adj}^{inv NEE} = F_{ML}^{inv NEE} - F_{ML}^{rivers} - F_{ant}^{crop trade} - F_{ant}^{wood trade} \Leftrightarrow F_{ant-nf}^{ni}, \quad (1)$$

where the sign  $\Leftrightarrow$  means 'compared with',  $F_{ant-nf}^{ni}$  is the non-fossil part of the anthropogenic CO<sub>2</sub> flux from NGHGs,  $F_{tot}^{rivers}$  is the sum of the natural and anthropogenic CO<sub>2</sub> flux on land from CO<sub>2</sub> fixation by plants that is leached as carbon via soils and channeled to inland waters to be exported to the ocean or to another country. All countries export river carbon, but some countries also receive river inputs, e.g., Romania receives carbon from Serbia via the Danube River. We estimated the lateral

40 carbon export by rivers minus the imports from rivers entering each country, including dissolved organic carbon, particulate  
41 organic carbon and dissolved inorganic carbon of atmospheric origin distinguished from lithogenic, by using the data and  
42 methodology described by Ciais et al. (2021). Data are from Mayorga et al. (2010) and Hartmann et al. (2009) and follow the  
43 approach of Ciais et al. (2021) proposed for large regions. We also extracted the lateral flux by rivers over the managed land  
44 by using the same methodology as inversion CO<sub>2</sub> flux. Thus, in a country that only exports river carbon to the ocean, the  
45 amount of carbon exported is equivalent to an atmospheric CO<sub>2</sub> sink, denoted as  $F_{ML}^{rivers}$  as in eq. (1), thus ignoring burial,  
46 which is a small term. Over a country that receives carbon from rivers flowing into its territory, a small national CO<sub>2</sub> outgassing  
47 is produced by a fraction of this imported flux. In that case, we assumed that the fraction of outgassed to incoming river carbon  
48 is equal to the fraction of outgassed to soil-leached carbon in the RECCAP2 region to which a country belongs, estimated with  
49 data from Ciais et al. (2021).

50  $F_{ant}^{crop\ trade}$  is the sum of CO<sub>2</sub> sinks and sources induced by the trade of crop products. This flux was estimated from the annual  
51 trade balance of crop commodities calculated for each country from data from the United Nations Statistics Division of the  
52 Food and Agriculture Organization (FAOSTAT) combined with the carbon content values of each commodity (Xu et al., 2021;  
53 [FAO, 2024](#)). All the traded carbon in crop commodities is assumed to be oxidized as CO<sub>2</sub> in one year, neglecting stock changes  
54 of products, and the fraction of carbon from crop products going to waste pools and sewage waters after consumption, thus  
55 not necessarily oxidized to atmospheric CO<sub>2</sub>.  $F_{ant}^{wood\ trade}$  is the sum of CO<sub>2</sub> sinks and sources induced by the trade of wood  
56 products (Zscheischler et al., 2017). Here, we followed Ciais et al. (2021) who used a bookkeeping model to calculate the  
57 fraction of domestically produced and imported carbon in wood products that are oxidized in each country during subsequent  
58 years, with product lifetimes defined by Mason Earles et al (2012) and encompassing all products (including roundwood and  
59 processed products). The underlying assumption in estimating CO<sub>2</sub> fluxes from wood harvest is that the emissions from  
60 domestically harvested wood, in addition to imported wood minus exported wood that is not allocated to wood product pools,  
61 are released into the atmosphere during the year of harvest. Conversely, wood allocated to wood product pools is gradually  
62 released into the atmosphere over time, based on their respective lifetimes. Domestic harvest is assumed to be balanced by an  
63 atmospheric CO<sub>2</sub> sink of equivalent magnitude, which is not necessarily the case given that harvest is rarely in equilibrium  
64 with forest increment, but inversions NEE will correct for this imbalance in our results, and can thus be compared with  
65 NGHGs. We included in the  $F_{ant}^{crop\ trade}$  flux the emissions of CO<sub>2</sub> by domestic animals consuming specific crop products  
66 delivered as feed. On the other hand, emissions of CO<sub>2</sub> from grazing animals and the decomposition of their manure are  
67 supposed to occur in the same grid box where grass is grazed, so that the CO<sub>2</sub> net flux captured by an inversion is comparable  
68 with grazed grasslands' carbon stock changes of inventories. Emissions of reduced carbon compounds (VOCs, CH<sub>4</sub>, CO) are  
69 not included in this analysis (see Ciais et al. (2021) for a discussion of their importance in inversion CO<sub>2</sub> budgets).

70 In summary, the purpose of the adjustment of eq. (1) is to make inversion output comparable to the NGHGs that do not include  
71  $F_{ML}^{rivers}$ ,  $F_{ant}^{crop\ trade}$  and  $F_{ant}^{wood\ trade}$ . The UNFCCC accounting rules (IPCC, 2006) assume that all the harvested wood  
72 products are emitted in the territory of a country that produces them, which is equivalent to ignoring  $F_{ant}^{wood\ trade}$  as a national

73 sink or source of CO<sub>2</sub>, hence the need to remove  $F_{ant}^{wood\ trade}$  from inversion NEE. The adjusted inversion fluxes from eq. (1)  
 74 depict the national CO<sub>2</sub> stock change which match better the carbon accounting system boundaries of UNFCCC NGHGs. In  
 75 the following, we will only discuss adjusted inversion CO<sub>2</sub> fluxes ( $F_{adj}^{inv\ NEE}$ ), but for simplicity call them “inversion fluxes”.

#### 76 2.4 Processing of CH<sub>4</sub> inversions for comparison with national inventories

77 Most atmospheric inversions derive total net CH<sub>4</sub> emissions at the surface as it is difficult for them to disentangle overlapping  
 78 emissions from different sectors at the pixel/regional scale based on atmospheric CH<sub>4</sub> observations only. However, five of the  
 79 seven inverse systems solve for some source categories owing to different spatio-temporal distributions between the sectors.  
 80 For each inversion, monthly gridded posterior flux estimates were provided at 1°x1° grid resolution for the net flux at the  
 81 surface ( $E_{net}^{inv}$ ), the soil uptake at the surface ( $E_{soil}^{inv}$ ), the total emission at the surface ( $E_{tot}^{inv}$ ) and five emitting ‘super sectors’  
 82 which regroup several IPCC sectors: Agriculture & Waste ( $E_{AgW}^{inv}$ ), Fossil Fuel ( $E_{FF}^{inv}$ ), Biomass & Biofuel Burning ( $E_{BB}^{inv}$ ),  
 83 Wetlands ( $E_{Wet}^{inv}$ ), and Other Natural ( $E_{Oth}^{inv}$ ) emissions. Considering the soil uptake as a ‘negative source’ given separately, the  
 84 following equations apply:

$$85 E_{net}^{inv} = E_{tot}^{inv} + E_{soil}^{inv} = E_{AgW}^{inv} + E_{FF}^{inv} + E_{BB}^{inv} + E_{Wet}^{inv} + E_{Oth}^{inv} + E_{soil}^{inv} \quad (2)$$

86 For inversions solving for net emissions only, the partition to source sectors was created based on using a fixed ratio of sources  
 87 calculated from prior flux information at the pixel scale. For inversions solving for some categories, a similar approach was  
 88 used to partition the solved categories to the five aforementioned emitting sectors. Such processing can lead to significant  
 89 uncertainties if not all sources increase or change at the same rate in a given region/pixel. National values have been estimated  
 90 using the country land mask described in the CO<sub>2</sub> section, thus offshore emissions are not counted as part of inversion results  
 91 unless they are in a coastal grid cell.

92 In our previous study (Deng et al., 2022), four methods were proposed to separate CH<sub>4</sub> anthropogenic emissions from  
 93 inversions ( $E_{Anth}^{inv}$ ) to compare them with national inventories ( $E_{Anth}^i$ ) aiming to discuss the uncertainties in anthropogenic  
 94 CH<sub>4</sub> emissions associated with the chosen separation methods. These four methods include: (1) summing prior estimates based  
 95 on inversions for anthropogenic sectors (method 1); (2) subtracting natural emissions from total fluxes (method 2); and (3)  
 96 subtracting natural emissions derived from other bottom-up assessments from the total inversion flux (methods 3/1 and 3/2,  
 97 differing only in the bottom-up wetland CH<sub>4</sub> data used). The calculations of anthropogenic emissions by each method were  
 98 performed separately for GOSAT inversions and in-situ inversions. However, the uncertainty from the separation method is  
 99 generally much smaller than the variability between different inversion models (see Deng et al. (2022) Fig 9). Therefore, we  
 00 apply only one method in this study which consists of using inversion partitioning as defined in Saunio et al. (2020):

$$01 E_{Anth}^{inv} = E_{AgW}^{inv} + E_{FF}^{inv} + E_{BB}^{inv} - E_{wildfires}^{BU} \Leftrightarrow E_{Anth}^i \quad (3)$$

02 This method has some uncertainties. First, the partitioning relies on prior fractions within each pixel, and second, emissions  
 03 from wildfires are counted for in the Biomass and Biofuel burning (BB) inversion category while they are not necessarily  
 04 reported in NGHGs. The BB inversion category includes methane emissions from wildfires in forests, savannahs, grasslands,

05 peats, agricultural residues, and the burning of biofuels in the residential sector (stoves, boilers, fireplaces). Therefore, we  
06 subtracted bottom-up (BU) emissions from wildfires ( $E_{wildfires}^{BU}$ ) based on the GFEDv4 dataset (van Wees et al., 2022) using  
07 their reported dry matter burned and CH<sub>4</sub> emission factors. Because the GFEDv4 dataset also reports specific agricultural and  
08 waste fire emissions data, we assumed that those fires (on managed lands) are reported by NGHGs, so they were not counted  
09 in  $E_{wildfires}^{BU}$ . Figure S3 presents a comparison between our adjusted BB flux and the wood fuel emissions reported by [Flammini](#)  
10 et al. (2023). This comparison highlights the broader scope and definition of our adjusted BB flux, illustrating the differences  
11 in emissions estimation methodologies.

删除了: Flammi

## 12 2.5 Processing of N<sub>2</sub>O inversions for comparison with inventories

13 We subtracted estimates of natural N<sub>2</sub>O sources from the N<sub>2</sub>O emission budget ( $E_{tot}^{inv}$ ) of each inversion, to provide inversions  
14 of anthropogenic emissions ( $E_{ant}^{inv}$ ) that can be compared with national inventories ( $E_{ant}^{ni}$ ):

$$15 E_{ant}^{inv} = E_{ML}^{inv} - E_{nat}^{aq} - E_{wildfires}^{GFED} \Leftrightarrow E_{ant}^{ni} \quad (4)$$

16 Here, the natural N<sub>2</sub>O sources include natural emission from freshwater systems ( $E_{nat}^{aq}$ ) and natural emissions from wildfires  
17 ( $E_{ant}^{ni}$ ).

18 In our previous study, intact forest grid cells (assumed unmanaged) from Potapov et al. (2017) and lightly grazed grassland  
19 areas from Chang et al. (2021) were removed from the gridded N<sub>2</sub>O emissions in proportion to their presence in each inversion  
20 grid box. Here we used the new managed land mask defined in **Section 2.3** to filter gridded N<sub>2</sub>O emissions from inversions to  
21 obtain  $E_{ML}^{inv}$ . We verified that the inversion grid box fractions classified as unmanaged do not contain point source emissions  
22 from the industry, energy, and diffuse emissions from the waste sector, to make sure that we do not inadvertently remove  
23 anthropogenic sources by masking unmanaged pixels. From the EDGARv4.3.2 inventory (Janssens-Maenhout et al., 2019),  
24 we found that N<sub>2</sub>O from wastewater handling covers a relatively large area that might be partly located in unmanaged land.  
25 But the corresponding emission rates are more than 1 order of magnitude smaller than those from agricultural soils. For other  
26 sectors, only very few of the unmanaged grid boxes contain point sources, and none of them have an emission rate that is  
27 comparable with agricultural soils (managed land). Thus, our assumption that emissions from these other anthropogenic sectors  
28 are primarily over managed land pixels is solid (other sectors include: the power industry; oil refineries and transformation  
29 industry; combustion for manufacturing; aviation; road transportation no resuspension; railways, pipelines, off-road transport;  
30 shipping; energy for buildings; chemical processes; solvents and products use; solid waste incineration; wastewater handling;  
31 solid waste landfills).

32 The flux  $E_{nat}^{aq}$  is the natural emission from freshwater systems given by a gridded simulation of the DLEM model (Yao et al.,  
33 2019) describing pre-industrial N<sub>2</sub>O emissions from N leached by soils and lost to the atmosphere by rivers in the absence of  
34 anthropogenic perturbations (considered as the average of 1900-1910). Natural emissions from lakes were estimated only at a  
35 global scale by Tian et al. (2020), and represent a small fraction of rivers' emissions. Therefore, they are neglected in this  
36 study. The flux  $E_{wildfires}^{GFED}$  is based on the GFED4s dataset (van Wees et al., 2022) using their reported dry matter burned and

38 N<sub>2</sub>O emission factors. Because the GFED dataset reports specific agricultural and waste fire emissions data, we assume that  
39 those fires (on managed lands) are reported by NGHGs so they were not counted in  $E_{wildfires}^{GFED}$  just like for CH<sub>4</sub> emissions.  
40 Note that there could also be a background natural N<sub>2</sub>O emission from natural soils over managed lands ( $E_{managed\ land}^{soil}$ ) which  
41 is not necessarily reported by NGHGs. We did not try to subtract this flux from managed land emissions because we assumed  
42 that, after a land use change from natural to fertilized agricultural land, background emissions decrease and become very small  
43 compared to N-fertilizers induced anthropogenic emissions. In a future study, we could use for  $E_{managed\ land}^{soil}$  the estimate  
44 given by simulations of pre-industrial N<sub>2</sub>O emissions from the NMIP ensemble of dynamic vegetation models with carbon-  
45 nitrogen interactions (number of models; n = 7). Namely, their simulation S0 in which climate forcing is recycled from 1901-  
46 1920; CO<sub>2</sub> is at the level of 1860, and no anthropogenic nitrogen is added to terrestrial ecosystems (Tian et al., 2019).  
47 Another important point to ensure a rigorous comparison between inversion and NGHGI data is whether anthropogenic indirect  
48 emissions (AIE) of N<sub>2</sub>O are reported in NGHGI reports. This is not always the case even though UNFCCC parties are required  
49 to report these in their NGHGs according to the IPCC guidelines. For example, South Africa's BUR3 did not report indirect  
50 N<sub>2</sub>O emissions due to the lack of activity data. AIE arise from anthropogenic nitrogen from fertilizers leached to rivers and  
51 anthropogenic nitrogen deposited from the atmosphere to soils. AIEs represent typically 20% of direct anthropogenic emissions  
52 and cannot be ignored in a comparison with inversions. For Annex I countries, AIEs are systematically reported, generally  
53 based on emission factors since these fluxes cannot be directly measured, and we assumed that indirect emissions only occur  
54 on managed land. For non-Annex I countries, we checked manually from the original NC and BUR documents if AIE was  
55 reported or not by each non-Annex I country. If AIEs were reported by a country, they were used as such to compare NGHGI  
56 data with inversion results, and grouped into the agricultural sector. If they were not reported, or if their values were outside  
57 plausible ranges, AIE were independently estimated by the perturbation simulation of N fertilizers leaching, CO<sub>2</sub> and climate  
58 on rivers and lakes fluxes in the DLEM model (Yao et al., 2019), and by the perturbation simulation of atmospheric nitrogen  
59 deposition on N<sub>2</sub>O fluxes from the NMIP model ensemble (Tian et al., 2019).

## 60 2.6 Grouping sectors for comparison

61 The bottom-up NGHGs are compiled based on activity data (statistics) following the IPCC 1996/2006 Guidelines (IPCC,  
62 1997, 2006) with detailed information on subsectors. However, the top-down inversions can only distinguish between very  
63 few groups of sectors at most. Thus, in this study, we aggregated NGHGI sectors into some 'super sectors' to make inversions  
64 and inventories comparable for each GHG (Table 2). For CO<sub>2</sub>, the inversions are divided into two aggregated super-sectors:  
65 fossil fuel and cement CO<sub>2</sub> emissions, and adjusted net land flux. Inversions use a prior gridded fossil fuel dataset as  
66 summarized in Section 1.2, thus, in this study, we compare only the net land flux between inversions and inventories. To  
67 calculate the net land flux over managed lands from NGHGs, we subtracted fossil emissions from the IPCC/CRF 1. Energy  
68 and 2. Industrial Processes (or 2. Industrial Processes and Product Use) sectors from the Total GHG emissions including  
69 LULUCF/LUCF (or Total national emissions and removals) sector. For CH<sub>4</sub>, we compare inversions and inventories based on

three super sectors, including *Fossil, Agriculture and Waste*, and *Total Anthropogenic*. To compare with NGHGs, we group the IPCC/CRF sectors of *1. Energy* and *2. Industrial Processes* (or *2. Industrial Processes and Product Use*) by excluding Biofuel Burning (reported under *1. Energy* sector) into the super sector of *Fossil*; we group sectors of *4. Agriculture* (or *3. Agriculture*) and *6. Waste* (or *5. Waste*) into the super sector of *Agriculture and Waste*; and we aggregate anthropogenic flux from *Fossil* and *Agriculture and Waste* and *Biofuel Burning* into *Anthropogenic*. For N<sub>2</sub>O, we grouped the NGHGI sectors into *Anthropogenic* flux being the sum of *1. Energy* + *2. Industrial Processes* (or *2. Industrial Processes and Product Use*) + *4. Agriculture* (or *3. Agriculture*) + *6. Waste* (or *5. Waste*) + *Anthropogenic Indirect Emissions*.

**Table 2. Grouping of NGHGs sectors into aggregated 'super-sectors' for comparisons with inversions.** \* Biofuel burning is likely not included in NGHGs but under *1.A.4 Other Sectors* if it is reported. \*\* Field burning of agricultural residues is reported in Annex I countries under the Agricultural sector. Note that indirect N<sub>2</sub>O emissions are reported by Annex I countries but not systematically by non-Annex I ones

Gas	Super-Sectors	Inversions	NGHGs (IPCC/CRF)
CO <sub>2</sub>	<i>Net Land (adjusted)</i> <i>Flux</i>	<i>Total - Fossil - lateral C</i>	Non-Annex I (IPCC): <i>Total GHG emissions including LULUCF/LUCF - (Energy + Industrial Processes)</i>  Annex I (CRF): <i>Total national emissions and removals - (Energy + Industrial Processes and Product Use)</i>
CH <sub>4</sub>	<i>Anthropogenic</i>	<i>Fossil + Agriculture &amp; Waste + Biofuel Burning</i>	Energy + Industrial Processes + Agriculture + Waste + Biofuel Burning*
	<i>Fossil</i>	<i>Fossil</i>	Energy + Industrial Processes - Biofuel Burning*
	<i>Agriculture and Waste</i>	<i>Agriculture &amp; Waste</i>	Agriculture + Waste - Field burning of agricultural residues**
N <sub>2</sub> O	<i>Anthropogenic</i>	<i>Total - pre-industrial inland waters</i>	Agriculture + Waste direct + anthropogenic indirect emissions (AIE = anthropogenic N leached to inland waters + anthropogenic N deposited from atmosphere) + energy and industry

81 **2.7 Choice of example countries for analysis**

82 For the analysis, we selected 12 countries (or groups of countries) based on specific criteria for each aggregated sector. Firstly,  
83 each chosen country had to possess a sufficiently large land area, as the limitations of coarse-spatial-resolution inversions  
84 make it difficult to reliably estimate GHG budgets for smaller countries. Additionally, it was preferable for the selected  
85 countries to have some coverage provided by the in situ global network of monitoring stations.

86 For CO<sub>2</sub>, we focus on the land CO<sub>2</sub> fluxes of large fossil fuel CO<sub>2</sub> emitters. Although inversions do not allow to verify fossil  
87 emissions in these countries as they are used as a fixed prior map of emissions, it is crucial to compare the magnitude of  
88 national land CO<sub>2</sub> sinks with fossil fuel CO<sub>2</sub> emissions in those large emitters. It is important to note that fitting net fluxes to  
89 changes in atmospheric CO<sub>2</sub> and then subtracting the prior fossil fuel (FF) fluxes can result in errors in the residual values,  
90 which are typically attributed exclusively to the sum of all non-FF fluxes. Additionally, we included two large boreal forested  
91 countries (Russia - RUS and Canada - CAN), two tropical countries with large forest areas (Brazil - BRA and the Democratic  
92 Republic of Congo - COD), two large countries with ground-based stations (Mongolia - MNG and Kazakhstan - KAZ), and  
93 two large dry Southern Hemisphere countries also with high rankings in fossil fuel CO<sub>2</sub> emissions (South Africa - ZAF and  
94 Australia - AUS), both of which possess atmospheric stations to constrain their land CO<sub>2</sub> flux.

95 For CH<sub>4</sub>, we first ranked countries (or groups of countries) based on their total anthropogenic, fossil, and agricultural emissions.  
96 This study includes China (CHN), India (IND), the United States (USA), the European Union (EUR), Russia (RUS), Argentina  
97 (ARG) and Indonesia (IDN), all of which are among the top emitters of both fossil fuel and agricultural CH<sub>4</sub> and possess large  
98 areas. Criteria of large land areas and the presence of atmospheric stations is crucial for in situ inversions. The advantage of  
99 utilizing GOSAT in CH<sub>4</sub> atmospheric inversions is its ability to provide observations over countries where surface in-situ data  
00 are sparse or absent, such as in the tropics. This allows us to consider countries with limited or few ground-based observations.  
01 Small countries were excluded due to the coarse spatial resolution. However, among the selected countries, Venezuela, with  
02 an area of 916,400 km<sup>2</sup>, was chosen specifically for the analysis of CH<sub>4</sub> emissions. Despite being relatively small, Venezuela  
03 is a large producer of oil and gas, potentially allowing for inversions using GOSAT satellite observations to constrain its  
04 emissions. In major oil- and gas-extracting countries that have negligible agricultural and wetland emissions like Kazakhstan  
05 (KAZ), grouped in this study with Turkmenistan (TKM) into KAZ&TKM; Iran (IRN); and Persian Gulf countries (GULF),  
06 fossil emissions should be easier to separate by inversions and thus to be compared with NGHGs.

07 For N<sub>2</sub>O, we selected the top 12 emitters based on the NGHGs reports. Anthropogenic N<sub>2</sub>O emissions in most of these  
08 countries are predominantly driven by the agricultural sector, which accounts for a share (including indirect emissions) ranging  
09 from 6% in Venezuela (VEN) to 95% in Brazil (BRA) of their total NGHGs emissions.

10 Together, the selected countries (or groups of countries) with a different selection for each gas, account for more than 90% of  
11 the global land CO<sub>2</sub> sink, 60% of the global anthropogenic CH<sub>4</sub> emissions (around 15% of fossil fuel emissions and  
12 approximately 40% of agriculture and waste emissions separately), and 55% of the global anthropogenic N<sub>2</sub>O emissions, as  
13 estimated by the NGHGs.

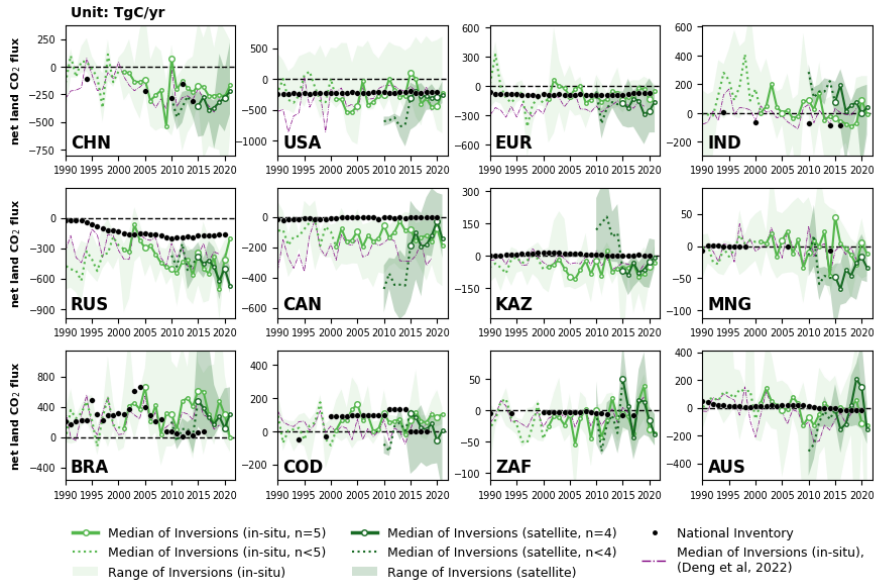
设置了格式: 下标



.14 **Table 3. Lists of countries or groups of countries are analyzed and displayed in the result section for each aggregated sector.**  
.15 Argentina (ARG), Australia (AUS), BRA (Brazil), Bangladesh (BGD), Canada (CAN), China (CHN), Columbia (COL), Democratic  
.16 Republic of the Congo (COD), Indonesia (IDN), India (IND), Iran (IRN), European Union (EUR), Kazakhstan (KAZ), Mexico (MEX),  
.17 Mongolia (MNG), Nigeria (NGA), Pakistan (PAK), Russia (RUS), South Africa (ZAF), Sudan (SDN), Thailand (THA), United States (USA),  
.18 Venezuela (VEN), GULF = Saudi Arabia + Oman + United Arab Emirates + Kuwait + Bahrain + Iraq + Qatar, KAZ&TKM = Kazakhstan  
.19 + Turkmenistan. For CH<sub>4</sub>, acronyms underlined denotes the countries appear in both *Anthropogenic* and *Fossil* or *Agriculture and Waste*  
.20 sectors.

Gas	Super Sector	Country List
CO <sub>2</sub>	<i>Net Land Flux</i>	AUS, BRA, CAN, CHN, COD, EUR, IND, KAZ, MNG, RUS, USA, ZAF
CH <sub>4</sub>	<i>Anthropogenic</i>	<u>ARG</u> , AUS, <u>BRA</u> , <u>CHN</u> , <u>EUR</u> , <u>IDN</u> , <u>IND</u> , <u>IRN</u> , <u>MEX</u> , <u>PAK</u> , <u>RUS</u> , <u>USA</u>
	<i>Fossil</i>	<u>CHN</u> , <u>EUR</u> , GULF, <u>IDN</u> , <u>IND</u> , <u>IRN</u> , KAZ&TKM, <u>MEX</u> , NGA, <u>RUS</u> , <u>USA</u> , VEN
	<i>Agriculture and Waste</i>	<u>ARG</u> , BGD, <u>BRA</u> , <u>CHN</u> , <u>EUR</u> , <u>IDN</u> , <u>IND</u> , <u>MEX</u> , <u>PAK</u> , <u>RUS</u> , THA, <u>USA</u>
N <sub>2</sub> O	<i>Anthropogenic</i>	AUS, BRA, CHN, COD, COL, EUR, IDN, IND, MEX, SDN, USA, VEN

21 **3 Results for net land CO<sub>2</sub> fluxes**



22  
 23 Figure 3 | Net land CO<sub>2</sub> fluxes (unit: TgC yr<sup>-1</sup>) during 1990-2021 from China (CHN), United States (USA), European Union  
 24 (EUR), Russia (RUS), Canada (CAN), Kazakhstan (KAZ), Mongolia (MNG), India (IND), Brazil (BRA), Democratic  
 25 Republic of the Congo (COD), South Africa (ZAF), and Australia (AUS). By convention, CO<sub>2</sub> removals from the atmosphere  
 26 are counted negatively, while CO<sub>2</sub> emissions are counted positively. The black dots denote the reported values from NGHGs.  
 27 The light green color denotes the in-situ-alone CO<sub>2</sub> inversion (n=5) set while the dark green color denotes the set that uses  
 28 satellite data (n=4). The green lines denote the median of land fluxes over managed land of CO<sub>2</sub> inversions, after adjustment  
 29 of CO<sub>2</sub> fluxes from lateral transport by rivers, crop, and wood trade. When all inverse models within the inversion sets (in-situ:  
 30 n=5; satellite: n=4) have available data for the same time interval, their median values are depicted as solid green lines.  
 31 Otherwise, when the inversion sets have incomplete inverse models within the time interval (in-situ: n<5; satellite: n<4), their  
 32 median values are represented as dashed green lines. Besides, before 2015, only GOSAT was available for the 2 of 4 satellite-  
 33 based inversions, until September 2014 when the OCO-2 record started. The shading area denotes the min-max range of  
 34 inversions. The purple dashed lines denote the median of inversions presented by the previous study (Deng et al., 2022).  
 35

设置了格式: 下标

设置了格式: 下标

设置了格式: 下标

设置了格式: 下标

设置了格式: 下标

设置了格式: 下标

.36 **Fig 3** presents the time series of land-to-atmosphere CO<sub>2</sub> fluxes for the selected countries listed in **Table 2**. The median of  
 .37 inversions across the 12 countries shows significant interannual variability, reflecting the impact of climate variability on  
 .38 terrestrial carbon fluxes and annual variations of land-use emissions. In this paper, for inversion results covering a time interval,  
 .39 we present the data as mean ± standard deviation, where the mean is the multi-year average of the median flux values from the  
 .40 inversion models, and the standard deviation represents the interannual variability.  
 .41 The adjustments of lateral CO<sub>2</sub> flux generally tend to lower land carbon sinks or increase land carbon emissions, especially in  
 .42 China (CHN), United States (USA), European Union (EUR), Russia (RUS), Canada (CAN), India (IND), and Brazil (BRA).  
 .43 In these countries, adjusting inversions by CO<sub>2</sub> fluxes induced by river carbon transport and by the trade of crop and wood  
 .44 products tends to lower CO<sub>2</sub> sinks, especially for large crop exporters like the USA and CAN. The adjusted net lateral transport  
 .45 fluxes for these countries are 48 (CHN), 143 (USA), 86 (EUR), 63 (RUS), 72 (CAN), 75 (IND), and 145 (BRA) TgC/yr, which  
 .46 represent 20%, 38%, 48%, 11%, 41%, 94%, and 60% of the managed land CO<sub>2</sub> fluxes before lateral transport adjustments,  
 .47 respectively. However, even with these adjustments, in countries of temperate latitudes, the median values of the five in-situ-  
 .48 alone inversion ensemble all indicate a net carbon sink during the 2010s, such as CHN with a sink of 180 ± 100 TgC/yr, USA  
 .49 (210 ± 180 TgC/yr), EUR (90 ± 50 TgC/yr), RUS (490 ± 100 TgC/yr) and CAN (110 ± 40 TgC/yr). In CHN, despite only 5  
 .50 reported values to UNFCCC, NGHGs show a good agreement with the inversion results, with both NGHGs and inversions  
 .51 exhibiting an overall increase in carbon sink over the study period. However, during 2015-2021, the median values of the  
 .52 satellite-based inversion ensemble show a higher carbon sink of 320 ± 60 TgC/yr than those from in-situ inversion results (220  
 .53 ± 50 TgC/yr) in CHN. In IND, there are also only five reported estimates from the NGHGs. The in-situ inversion results  
 .54 indicate that India exhibited fluctuations between being a carbon source and a carbon sink during the period of 2001-2014 (40  
 .55 ± 70 TgC/yr). During 2015-2019, the in-situ inversion results in IND show a median carbon sink of 65 ± 20 TgC/yr, however,  
 .56 the median reverted to being a carbon source of 90 TgC/yr (ranging from a sink of 350 to a source of 260) in 2020. In contrast,  
 .57 the median values of satellite-based inversion ensemble indicate a carbon source of 65 ± 64 TgC/yr during 2015-2021 in IND.  
 .58 As Annex I countries, USA, EUR, RUS, CAN, and Kazakhstan (KAZ) have continuously reported annual NGHGs since 1990.  
 .59 The NGHGs reported values for the USA and CAN indicate a decline trend (Mann-Kendall Z=-0.6, p<0.01) of carbon sinks  
 .60 by an annual average rate of 0.7 TgC/yr<sup>2</sup> and 0.5 TgC/yr<sup>2</sup>. Like in Deng et al. 2022, we found that the carbon sink of Canada's  
 .61 managed land is significantly larger (-130 ± 50 TgC/yr over 2001-2021 from in-situ inversions) than the NGHGs reports (5 ±  
 .62 4 TgC/yr over 2001-2021). Part of this difference could be due to the fact that Canada decides in its inventory not to report  
 .63 fire emissions as they are considered to have a natural cause. Doing so, Canada also excludes recovery sinks after burning and  
 .64 those recovery sinks could surpass on average fire emissions, although remote sensing estimates of post fire biomass  
 .65 changes suggest that fire emissions have exceeded regrowth on average in Western Canada  
 .66 and Alaska until ≈ 2010 (Wang et al., 2021). One reason for the difference may be that the NGHGI used old growth  
 .67 curves for forests, potentially underestimating the actual forest growth. Another reason for the difference may be shrubland  
 .68 and natural peatland carbon uptake and possibly an underestimated increase of soil carbon in the national inventory. For the

设置了格式: 字体: 加粗

设置了格式: 下标

设置了格式: 字体: 加粗

设置了格式: 下标

设置了格式: 下标

设置了格式: 下标

删除了: China

删除了: Russia

删除了: Canada

删除了: India

删除了: Brazil

设置了格式: 下标

删除了:

删除了: median

删除了: 1

设置了格式: 上标

设置了格式: 上标

删除了: 125

删除了: ± 45

删除了:

.80 USA we have a good agreement between inversions ( $-290 \pm 180$  TgC/yr for in-situ over 2001-2021) and the NGHGs data (-  
.81  $220 \pm 10$  TgC/yr over 2001-2021) with the inversion showing much more interannual variability, the US being a net source of  
.82 carbon in the years 2011, 2015 and 2016 from the median of in-situ inversions. The lower variability in the NGHGs data  
.83 reflects the 5-years averaging of C stock changes by the national forest inventory. In EUR, the new in-situ inversion ensemble  
.84 gives a lower carbon sink than the previous one (red line in Fig 3, see discussion in section 6.1), now being in good agreement  
.85 ( $-80 \pm 60$  TgC/yr) with NGHGs ( $-85 \pm 10$  TgC/yr) over 2001-2021. The OCO-2 satellite inversions give a higher sink than  
.86 in-situ inversions by  $-200 \pm 80$  TgC/yr, possibly because the in-situ surface network does not cover Eastern European countries  
.87 which have a larger NEE than Western European ones, whereas OCO-2 data have a more even coverage of the continent, as  
.88 discussed by Winkler et al. (2023), see their Fig. 2 showing that OCO-2 inversions have a similar NEE than in-situ ones in  
.89 Western Europe but a larger mean NEE uptake in Eastern Europe).

.90 In contrast, the NGHGs in RUS reports a rapid trend of increasing sink by a rate of  $4.6$  TgC/yr<sup>2</sup> (Mann-Kendall  $Z=0.69$ ,  
.91  $p<0.01$ ) during 1990-2020, supported by the significant strong correlation with the medians of in-situ inversion ensemble  
.92 ( $\rho=0.7$ ,  $p<0.01$ ) during 2001-2020. However, the median values for both the in-situ ( $480 \pm 100$  TgC/yr) and satellite-based  
.93 ( $450 \pm 90$  TgC/yr) inversion ensemble over RUS indicate larger larger land carbon sinks than those reported in the NGHGs  
.94 ( $180 \pm 10$  TgC/yr) during 2011-2020. For KAZ, the NGHGs suggest that managed land is a slight carbon source ( $6 \pm 5$  TgC/yr)  
.95 during 2000-2020. However, the median values for both satellite-based and in-situ inversion ensemble indicate a carbon sink  
.96 of  $50 \pm 30$  TgC/yr and  $60 \pm 30$  TgC/yr, respectively, during 2015-2021 and 2001-2021. It is worth noting that the satellite-based  
.97 inversion results for USA, CAN, and KAZ all exhibit shifts in their fluxes between 2010 and 2015 compared to the results  
.98 after 2015. This is attributed to the use of different satellite data and the number of different ensembles during these periods.  
.99 Before 2015, only GOSAT was available, and only 2 out of 4 systems were available. After the OCO-2 record started, in  
.00 September 2014, the satellite-driven inversion set only assimilated OCO-2. This indicates that inversion results based on  
.01 GOSAT data are not consistent at the country scale with OCO-2 inversions. As a result, we can compare OCO-2 inversions  
.02 with NGHGs since 2015, but not the trends from inversions using GOSAT and/or OCO-2 inversions since 2009.

.03 In BRA, both the NGHGs reports ( $240 \pm 170$  TgC/yr during 1990-2016) and inversion results (in-situ:  $350 \pm 190$  TgC/yr  
.04 during 2001-2021; satellite-based:  $280 \pm 120$  TgC/yr during 2015-2021) indicate that the country has been a net carbon source  
.05 since 1990. The carbon source from managed land in Brazil increased from the late 1990s, reaching a peak around 2005  
.06 according to NGHGs ( $677$  TgC/yr). This evolution is confirmed by in-situ inversions with a source peaking in 2005 ( $\sim 650$   
.07 TgC/yr). The net carbon source from inversions then decreased from 2005 to 2011, which is consistent with the observed  
.08 reduction in deforestation due to forest protection policies implemented by the Brazilian government. This is an encouraging  
.09 result as the inversions did not explicitly consider land use emissions in their prior assumptions, although some included an  
.10 estimate of carbon released by fires in their prior which is part of land-use emissions in Brazil. Since NEE is defined as all  
.11 land fluxes except fossil fuel emissions, NEE from all inversions nevertheless include land use emissions from deforestation,  
.12 degradation emissions and fire emissions including fires from deforestation, degradation and other fires. After 2011, inversions  
.13 show a new increase in land emissions, with a peak during the 2015-2016 El Niño. There have been higher average land

删除了: 75

删除了:  $\pm 60$

删除了: 5

删除了:

删除了:

删除了: 178

删除了: 11

删除了:  $53 \pm 29$

删除了:  $57 \pm 33$

删除了:  $239 \pm 166$

emissions thereafter. These ongoing changes may be attributed to various factors such as the legacy effects of drought leading to increased tree mortality (Aragão et al., 2018), higher wildfire emissions (Naus et al., 2022; Gatti et al., 2023), carbon losses from forest degradation, and climate change-induced reductions in forest growth due to regional drying and warming in the southern and eastern parts of the Amazon (Gatti et al., 2021). From 2011 to 2016, the NGHGs reports indicate that carbon emissions from Brazilian managed lands were stable at around 47 TgC/yr. However, the medians of in-situ inversions suggest that carbon emissions rapidly increased from ~100 TgC/yr in 2011 to ~600 TgC/yr in 2016, which peaked in 2015 (~610 TgC/yr). From 2016 to 2021, the medians for both in-situ and satellite inversion results show a decrease in carbon emissions from 2016 to 2018 but a transient peak in 2019, a year with large fires (Gatti et al., 2023) (in-situ: 480 TgC/yr; satellite: 270 TgC/yr). Then carbon emissions decreased again until 2021, which experienced wetter conditions and fewer fires (Peng et al., 2022); The in-situ inversion results show a continuous decrease to -10 TgC/yr in 2021, while the satellite inversion results showed a persistent source carbon anomaly of 300 TgC/yr. We emphasize moreover that available CO<sub>2</sub> observations from a network of aircraft vertical sampling (Gatti et al., 2021) were not used to constrain the inverse models used here.

For Democratic Republic of the Congo (COD), the available NGHGs data indicates that before 2000, the country's managed lands were a net carbon sink (50 TgC/yr in 1994 and 30 TgC/yr in 1999). Since 2000, the NGHGs reports indicated three stages of different levels of CO<sub>2</sub> flux, which COD managed land was a carbon source during 2000-2010 (-95 TgC/yr), a larger carbon source during 2011-2014 (-135 TgC/yr), and a very small sink during 2015-2018 (-1 TgC/yr). The medians of in-situ inversion ensemble indicate a similar annual average carbon source (70 ± 45 TgC/yr) during 2001-2021 with the NGHGs, despite the few observations over Africa (Byrne et al., 2023). In the recent decade, satellite inversion results from 2015 to 2021 indicate a smaller source (30 ± 55 TgC/yr) compared to the in-situ results (85 ± 25 TgC/yr). Moreover, the satellite inversion results indicate a sink anomaly in 2020 (-60 TgC/yr) which is not found in the in-situ inversions. The sink anomaly in 2020 from the satellite inversions is consistent with wetter conditions during that year over COD.

For South Africa (ZAF), the NGHGs show a stable very small sink of 3 TgC/yr during 1990-2010 that doubled from 4 TgC/yr in 2010 to 8 TgC/yr in 2017, while the in-situ inversion results indicate large fluctuations from a carbon sink (especially peaked in 2006, 2009, 2011, 2017 and 2021) to a small carbon source (e.g., in 2013, and 2018-2019). From 2015 to 2021, the satellite-based inversion results are consistent with the in-situ results for annual variability ( $\rho=0.8$ ,  $p<0.05$ ), which is a good sign of the consistency between different atmospheric observing systems. During the transition to El Niño conditions and drought from 2014 to 2015, however, the satellite-based inversion results indicate a switch from a carbon sink to a source anomaly of 50 TgC/yr in ZAF which is not seen in the in-situ inversions.

In Australia (AUS), the NGHGs data shows a land source of carbon from 1990 to 2012, which decreased over time (from 48 TgC/yr in 1990 to 1 TgC/yr in 2012) and changed into a carbon sink since 2013 (that increased from a sink of 1 TgC/yr in 2013 to 15 TgC/yr in 2020). However, the in-situ inversions indicate fluctuations between a carbon source and a sink with an annual average small sink of 10 ± 71 TgC/yr observed over the period of 2001-2021, except for 2009-2011, the medians of in-situ inversions reveal a strong carbon sink of 105 ± 35 TgC/yr. Between 2010 and the strong La Niña year of 2011, the medians of in-situ inversion ensemble from the previous study (Deng et al., 2022) showed an increase in carbon uptake of 145%. This

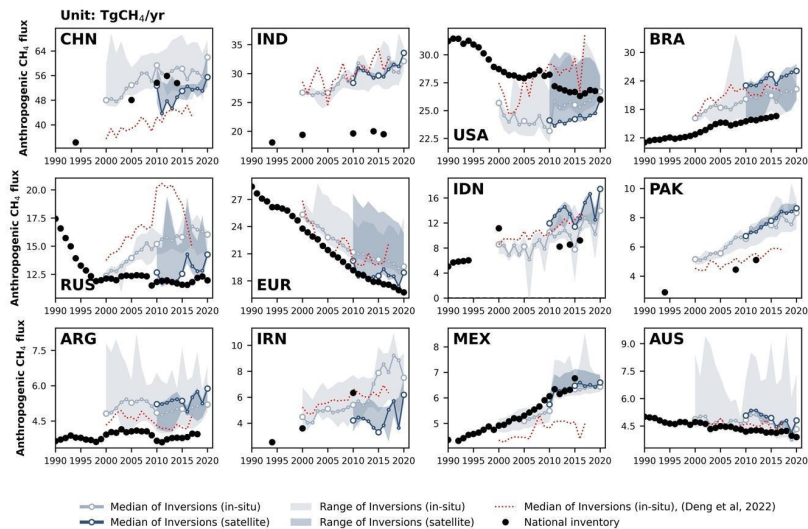
删除了: ± 0.5  
删除了: ± 0.1  
删除了: .2 ± 0.1

61 high carbon sink persisted in 2012, which was a dryer year with maximum bushfire activity. However, in this study, the  
62 medians of updated in-situ inversion ensemble indicate that there is a sink anomaly in 2011 followed by a source anomaly in  
63 2013, which appears to be more realistic. 2019 was the driest and hottest year recorded in Australia, including extreme fires at  
64 the end of 2019 (Byrne et al., 2021). As a result, the medians for both in-situ and satellite inversion ensemble show a carbon  
65 source anomaly in 2019, with 55 TgC/yr (ranging from a sink of 1060 to a source of 480) and 200 TgC/yr (ranging from a sink  
66 of 120 to a source of 320) respectively. When it comes to the wet La Niña year of 2021, the medians for both in-situ and  
67 satellite inversion ensemble indicate that AUS managed land became a carbon sink of 130 TgC/yr (ranging from a sink of  
68 1120 to a source of 25) and 150 TgC/yr (ranging from a sink of 260 to a source of 40).

69 Last, we give the global comparison between NGHGs and inversions, using NGHGs data compiled for all countries by Grassi  
70 et al. (2023) which include Annex I countries reports, non-Annex I NC, BUR and NDCs. The river correction is the only one  
71 that changes the global NEE, because the global mean of CO<sub>2</sub> fluxes from wood and crop products is close to zero. The river-  
72 induced CO<sub>2</sub> uptake over land that is removed from inversion NEE is equal to the C flux transported to the ocean at river  
73 mouths (0.9 GtC/yr in our estimate, close to the value of Regnier et al. 2022).The (in-situ) inversions without the river  
74 correction give a global NEE sink of 1.8 GtC/yr over 2001-2020, managed land: 1.3 GtC/yr (72% of total), unmanaged land:  
75 0.5 GtC/yr (28%). The in-situ inversions with the river correction study give a global NEE sink of 0.91 GtC/yr, managed  
76 land:0.51 GtC/yr (56% of total), unmanaged land 0.4 GtC/yr (44% of the total) This is an important update from Deng et al.  
77 2022 where the river CO<sub>2</sub> flux correction was not applied separately to managed / unmanaged lands. Because managed lands  
78 have a much larger area than unmanaged ones and because of the spatial patterns of the CO<sub>2</sub> sinks in the river correction are  
79 distributed with MODIS NPP which has low values in unmanaged lands of northern Canada and Russia, the river correction  
80 reduces strongly the C storage change with respect to NEE over managed lands, and marginally in unmanaged lands.. Inventory  
81 data recently compiled by Grassi et al. (2023) indicates a similar global land sink (on managed land) of 0.53 GtC yr<sup>-1</sup> with gap-  
82 filled data during the same period than the inversions with our improved river correction.

83 4 Results for anthropogenic CH<sub>4</sub> emissions

84 4.1 Total anthropogenic CH<sub>4</sub> emissions



85  
86 **Figure 4.** Total anthropogenic CH<sub>4</sub> fluxes for the 12 top emitters: China (CHN), India (IND), United States (USA), Brazil (BRA),  
87 Russia (RUS), European Union (EUR), Indonesia (IDN), Pakistan (PAK), Argentina (ARG), Iran (IRN), Mexico (MEX), and  
88 Australia (AUS). The black dots denote the reported values from NGHGs. The light and dark blue lines/areas denote the median and  
89 maximum-minimum ranges of in-situ and satellite-based CH<sub>4</sub> inversions based on EDGARv6.0 as the prior respectively.

90  
91 **Fig 4** presents the variations in anthropogenic CH<sub>4</sub> emissions for the 12 selected countries, where these emissions are summing  
92 the sectors of agriculture and waste, fossil fuels, and biofuel burning. The distribution of emissions is highly skewed even  
93 among the top 12 emitters, with the largest and most populated countries such as China (CHN), India (IND), United States  
94 (USA), Brazil (BRA), Russia (RUS), and European Union (EUR) which emits more than 10 TgCH<sub>4</sub>/yr annually, while other  
95 countries have smaller emissions (ranging from 3 to 10 CH<sub>4</sub>/yr) that are more challenging to quantify through inversions.  
96 During 2010-2020, CHN has the highest total anthropogenic emissions at around 50 ± 4 Tg CH<sub>4</sub>/yr, followed by IND with 30  
97 ± 1 Tg CH<sub>4</sub>/yr, USA with 24 ± 1 Tg CH<sub>4</sub>/yr, BRA with 24 ± 1 Tg CH<sub>4</sub>/yr, EUR with 19 ± 1 Tg CH<sub>4</sub>/yr, Indonesia (IDN) with  
98 14 ± 1 Tg CH<sub>4</sub>/yr and RUS with 13 ± 1 Tg CH<sub>4</sub>/yr, according to the medians of satellite-based inversion ensemble based on  
99 EDGARv6.0 as prior. The remaining countries have emissions of approximately 5 Tg CH<sub>4</sub>/yr. In general, the difference

- 删除了: 3.5
- 删除了: 1.4
- 删除了: 0.6
- 删除了: 1.2
- 删除了: 0.7
- 删除了: 0.9
- 删除了: 0.9

between NGHGs and inversions aligns in the same direction based on both satellite and in-situ inversions. This provides some confidence for using inversions to evaluate NGHGs as the satellite observations are independent from in situ networks. Overall, satellite-based inversions may be more robust across most countries due to better observation coverage, except in EUR and the USA where the in-situ network is more extensive.

Developing countries, such as CHN, IND, BRA, IDN, Pakistan (PAK), Iran (IRN) and Mexico (MEX), show a rapid increase in anthropogenic CH<sub>4</sub> emissions supported by reported values from NGHGs and results from inversions. In CHN, the reported values from NGHGs (when available) generally align with the results obtained through inversions (e.g., during 2010-2015, NGHGs:  $54 \pm 1 \text{ Tg CH}_4/\text{yr}$ , in-situ:  $58 \pm 1 \text{ Tg CH}_4/\text{yr}$ , satellite-based:  $48 \pm 3 \text{ Tg CH}_4/\text{yr}$ ). During 2010-2020, the median values for the in-situ and satellite-based inversion ensemble show a similar increase trend at an annual growth rate of  $0.28 \text{ Tg CH}_4/\text{yr}^2$  and  $0.26 \text{ Tg CH}_4/\text{yr}^2$  respectively, although the medians of in-situ inversion ensemble ( $58 \pm 2 \text{ Tg CH}_4/\text{yr}$ ) were slight higher than the satellite-based ensemble ( $50 \pm 3 \text{ Tg CH}_4/\text{yr}$ ). However, in 2020, the medians of the emission estimates for both in-situ and satellite-based inversions reveal a rapid increase by 9% and 11% compared to 2019 in CHN, indicating a possible surge in anthropogenic methane emissions for that year, possibly an artifact from the fact that the decreased OH sink in 2020 is not well accounted for here. Indeed OH interannual variability were not prescribed to all inversions, and when accounted for the OH interannual variability prescribed (based on Patra et al., 2021) was much smaller than those suggested by recent studies (e.g., Peng et al., 2022). As a result overestimating the sink in the inversions leads to overestimated surface emissions. The surge in emissions could also be due to spin-down, the last six month to one year of inversions being less constrained by the observations, even though the inversion period covered up to June 2021.

In IND, PAK and MEX, there is good agreement ( $r > 0.8$ ,  $p < 0.01$ ) between the in-situ and satellite-based inversion ensembles (respectively,  $31 \pm 1 \text{ Tg CH}_4/\text{yr}$  and  $30 \pm 1 \text{ Tg CH}_4/\text{yr}$  in IND,  $8 \pm 1 \text{ Tg CH}_4/\text{yr}$  and  $7 \pm 1 \text{ Tg CH}_4/\text{yr}$  in PAK, and  $6 \pm 1 \text{ Tg CH}_4/\text{yr}$  and  $6 \pm 1 \text{ Tg CH}_4/\text{yr}$  in MEX), while both of them present a significant increasing trend of anthropogenic methane emissions in these countries (Mann-Kendall  $p < 0.05$ ). However, when comparing to NGHGs values, the inversion results in IND and PAK indicate >50% larger emissions than the values reported from the NGHGs during 2010-2020. In contrast, values reported from the NGHGs ( $-6 \text{ Tg CH}_4/\text{yr}$ ) by MEX also show good agreement with the inversion results.

In BRA, IDN and Argentina (ARG), the medians for in-situ and satellite-based inversion ensembles show good consistency ( $r = 0.8$ ,  $p < 0.01$ ) in these two countries, while satellite-based inversion results are generally higher than the in-situ inversion results. Specifically, in BRA, the satellite-based inversions ( $24 \pm 1 \text{ Tg CH}_4/\text{yr}$ ) were 16% higher than the in-situ inversions ( $21 \pm 1 \text{ Tg CH}_4/\text{yr}$ ) and 52% higher than the NGHGs estimation ( $-17 \text{ Tg CH}_4/\text{yr}$ ) during 2010-2020, possibly owing to difficulties for inversions to separate between natural (wetlands, inland waters) and anthropogenic sources in this country, and possible flaws in the prior used for natural and anthropogenic fluxes. In IDN, NGHGs reported a significant continuous upward trend at an annual average growth of  $0.3 \text{ Tg CH}_4/\text{yr}$ , with a noticeable positive outlier in 2000. The medians for both in-situ and satellite-based inversion ensembles also indicate an upward trend in IDN, but both of them present sudden dips in anthropogenic methane emissions in 2015 and 2019 by 15-23% and 16-25%, compared to the previous year respectively. It is unlikely that anthropogenic activities could contribute such large year to year variations except for different flooded areas

删除了: .3

删除了: .2

删除了: .4

删除了: .0

删除了: .5

删除了: .2

删除了: .4

删除了: .07

删除了: .05

删除了: .02

删除了: .03

删除了:  $\pm 0.2$

删除了: 1.2

删除了: 0.8

删除了:  $\pm 0.4$



56 used for rice paddies. In ARG, the satellite-based inversion results also indicate two sudden dips in 2016 and 2019, however,  
57 such pattern was not found in the in-situ inversion results. A cause of year to year variations from inversions is the lack of in-  
58 situ sites and variable cloud cover affecting the density of GOSAT data.

59 Regarding IRN, NGHGs only provided data for three years (1994, 2000, and 2010), making it difficult to compare with  
60 inversion results. However, NGHGs show a rapid growth in anthropogenic CH<sub>4</sub> emissions (+9.4%/yr) during this period.  
61 There are significant differences between inversion results and for IRN, with satellite inversions generally giving lower  
62 emissions than in-situ inversions and different trends. Satellite inversions suggest a declining trend between 2010 and 2015,  
63 followed by a fluctuating increase until 2020. In contrast, in-situ-based inversions (by any nearby measurement stations, thus  
64 likely reflecting the prior trend) show a rapid rise in emissions after 2010, reaching a peak in 2018, followed by a decline.

65 NGHGs for RUS indicate that anthropogenic CH<sub>4</sub> emissions have been reduced during the 1990s and remained stable since  
66 2000 (12.0 ± 0.3 Tg CH<sub>4</sub>/yr during 2000-2020), which is similar with the trend observed from satellite-based inversion results  
67 (12.7 ± 0.9 Tg CH<sub>4</sub>/yr during 2000-2020). However, in 2016, there was a sudden increase of emissions in satellite inversion  
68 results (+14% increase from 12.5 Tg CH<sub>4</sub>/yr in 2015 to 14.2 Tg CH<sub>4</sub>/yr in 2016), followed by a gradual decline, and then a  
69 new increase in 2020 (+11% increase from 12.8 Tg CH<sub>4</sub>/yr in 2019 to 14.3 Tg CH<sub>4</sub>/yr in 2020). This recent change was not  
70 observed in the in-situ inversion results or the NGHGs.

71 For USA, Australia (AUS), and EUR, NGHGs reported a slow declining trend (EUR: 0.4 Tg CH<sub>4</sub>/yr; USA: 0.2 Tg CH<sub>4</sub>/yr;  
72 AUS: -0.04 Tg CH<sub>4</sub>/yr) in anthropogenic CH<sub>4</sub> emissions. In the case of the USA, inversion-derived emissions are slightly  
73 lower than NGHGs (in-situ-based: 9% lower during 2000-2020; satellite-based: 11% lower during 2010-2020). However,  
74 both ground-based and satellite-based inversions indicate that anthropogenic CH<sub>4</sub> emissions have remained relatively steady  
75 since 2000, without reflecting the slow decline reported by NGHGs. In EUR, NGHGs indicate that anthropogenic CH<sub>4</sub>  
76 emissions have been decreasing rapidly since 1990 (-1.4%/yr), consistent with the trend obtained from inversion results.  
77 However, in-situ inversion emissions are on average slightly higher than NGHGs, and this difference has been gradually  
78 increasing from 8% in the 2000s to 15% in the 2010s.

删除了:

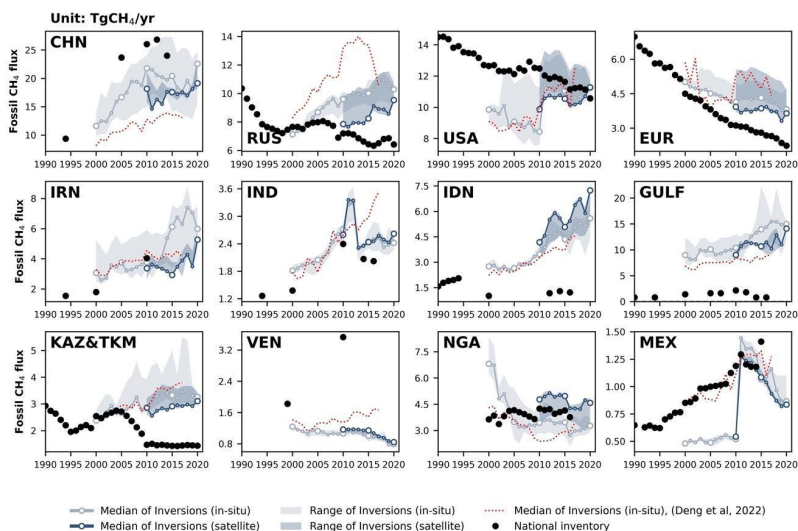
删除了: .3

删除了: .4

删除了: 7.7

删除了: 14.5

84 4.2 Fossil CH<sub>4</sub> emissions



85  
 86 **Figure 5.** CH<sub>4</sub> emissions from the fossil fuel sector from the top 12 emitters of this sector: China (CHN), Russia (RUS), United States  
 87 (USA), European Union (EUR), Iran (IRN), India (IND), Indonesia (IDN), Persian Gulf countries (GULF = Saudi Arabia + Iraq +  
 88 Kuwait + Oman + United Arab Emirates + Bahrain + Qatar), Kazakhstan & Turkmenistan (KAZ&TKM), Venezuela (VEN),  
 89 Nigeria (NGA), and Mexico (MEX). The black dots denote the reported value from the NGHGs. In the NGHGI data shown in Fig 5 for  
 90 GULF, Saudi Arabia reported four NGHGs in 1990, 2000, 2010, and 2012, Iraq reported one in 1997, Kuwait reported three in 1994, 2000,  
 91 and 2016, Oman reported one in 1994, United Arab Emirates reported four in 1994, 2000, 2005 and 2014, Bahrain reported three in 1994,  
 92 2000 and 2006, and Qatar reported one in 2007. The reported values are interpolated over the study period to be summed up and plotted in  
 93 the figure. For KAZ&TKM, the reported values of Turkmenistan during 2001-2003, 2005-2009, 2011-2020 are interpolated and added to  
 94 annual reports from Kazakhstan, an Annex I country for which annual data are available. Other lines, colors and symbols as Fig 4.

95 **Fig 5** presents the fossil CH<sub>4</sub> emissions for the top 12 emitters from the fossil sector based on EDGARv6.0 as the prior. The  
 96 largest emitter is China (CHN), mainly from the sub-sector of coal extraction, followed by Russia (RUS) and the United States  
 97 (USA). In CHN, the in-situ ( $20 \pm 2$  Tg CH<sub>4</sub>/yr) and satellite inversions ( $17 \pm 1$  Tg CH<sub>4</sub>/yr) emissions in the 2010s are 24% and  
 98 35% lower than in the NGHGs ( $\sim 26$  Tg CH<sub>4</sub>/yr), respectively. The NGHGs in CHN suggest a decrease from 28 in 2012 to  
 99 24 TgCH<sub>4</sub>/yr in 2014. However, both in-situ and satellite inversion results indicate an increasing trend since 2018. In India  
 100 (IND) and Indonesia (IDN), NGHGs report a decreasing trend during the study period, while inversions suggest a rapid  
 101 increase in IDN and a stable value in IND after a peak in 2012. In IND, satellite inversions suggest a peak of fossil CH<sub>4</sub>

删除了: 1.6

删除了: 1.3

删除了: ±

删除了: 2

删除了: 1.5

'07 emissions during 2011-2012, which then dropped in 2013 and remained stable afterward. In IDN, both in-situ and satellite  
'08 inversions indicate a fluctuating trend, with a significant drop between 2015 and 2019. In RUS, both in-situ and satellite  
'09 inversion-based estimates of fossil fuel emissions are higher than NGHGs, and show an increasing trend, while NGHGs  
'10 report a decreasing trend. This discrepancy may be due to inversion problems for separating between wetland emissions and  
'11 gas extraction industries both located in the Yamal peninsula area, or leaks not captured in NGHGs. In USA, NGHGs overall  
'12 show a significant declining trend (Mann-Kendall  $Z=-0.8$ ,  $p<0.01$ ). In-situ inversion estimates of fossil fuel emissions are 26%  
'13 lower than NGHGs during 2000-2010, and remained consistent until around 2011. Nearly all in-situ inversions show a jump  
'14 in fossil fuel emissions in 2011. In the European Union (EUR), both NGHGs and inversion results demonstrate a consistent  
'15 declining trend. However, starting from 2010, both in-situ and satellite inversions are higher than NGHGs reports.  
'16 Major oil-producing countries in the Persian Gulf are too small compared to the model resolution to be studied individually.  
'17 Hence, NGHGs from the GULF countries (Saudi Arabia, Iraq, Kuwait, Oman, United Arab Emirates, Bahrain, and Qatar)  
'18 were grouped and show much lower emissions compared to inversion results. In the 2010s, in-situ and satellite inversions  
'19 estimate that emissions in GULF were 9 times and 8 times higher than the estimates reported in NGHGs, respectively. This  
'20 huge under-reporting of emissions in GULF could be partly attributed to the omission of ultra-emitters in NGHGs. The ultra-  
'21 emitters defined by Lauvaux et al. (2022) are namely all short-duration leaks from oil and gas facilities (e.g., wells, compressors)  
'22 with an individual emission  $>20 \text{ t CH}_4/\text{h}$ , each event lasting generally less than one day. Such leaks are often random  
'23 occurrences and difficult to quantify, which is why most countries do not account for these significant and episodic events in  
'24 the national inventories. Indeed, recent studies by Lauvaux et al. (2022) have identified more ultra-emitters and larger emission  
'25 budgets from ultra-emitters in Qatar, Kuwait, and Iraq. In KAZ&TKM, grouped together because of their rather small  
'26 individual areas, both in-situ ( $3 \pm 0.2 \text{ Tg CH}_4/\text{yr}$ ) and satellite ( $3 \pm 0.1 \text{ Tg CH}_4/\text{yr}$ ) inversions estimate emissions to be 2 times  
'27 higher than NGHGs ( $1.5 \text{ Tg CH}_4/\text{yr}$ ) in the 2010s. Similarly, KAZ is located downwind of TKM, which has a high share of  
'28 ultra-emitters. The global inversions operating at a coarse resolution may misallocate emissions from TKM to KAZ. It is worth  
'29 noting that KAZ has two in-situ stations for  $\text{CH}_4$  measurements, whereas the GULF countries lack in-situ station networks.  
'30 On the other hand, the GOSAT satellite provides a dense sampling of atmospheric column  $\text{CH}_4$  in the Persian Gulf region due  
'31 to frequent cloud-free conditions. Therefore, GOSAT inversions can be considered more accurate than in-situ inversions for  
'32 Iran (IRN), GULF countries, and Kazakhstan & Turkmenistan (KAZ&TKM). Additionally, it is important to note that GOSAT  
'33 inversions generally give lower emissions than in-situ inversions in those countries. Venezuela (VEN) is a rare case where  
'34 NGHGs report much higher  $\text{CH}_4$  emissions than inversions. While the uncertainty of GOSAT inversions (model spread) has  
'35 decreased compared to the results reported by Deng et al. 2022, the gap between inversions and NGHGs has increased. In  
'36 2010, NGHGs reports of fossil  $\text{CH}_4$  emissions in VEN were 298% higher than GOSAT inversions and 326% than in-situ  
'37 inversions. We do not have a clear explanation for this large difference, except that VEN has strongly decreased oil and gas  
'38 extraction due to sanctions curbing its crude production from  $2.7 \text{ mb/d}$  in 2015 to  $0.6 \text{ mb/d}$  in 2020 (OPEC, 2023), which may  
'39 not be reflected in their NGHGs. In Nigeria (NGA) and Mexico (MEX), NGHGs estimates fall between the median of in-situ

删除了:

删除了: -1

设置了格式: 下标

删除了: .3

删除了: 2.9

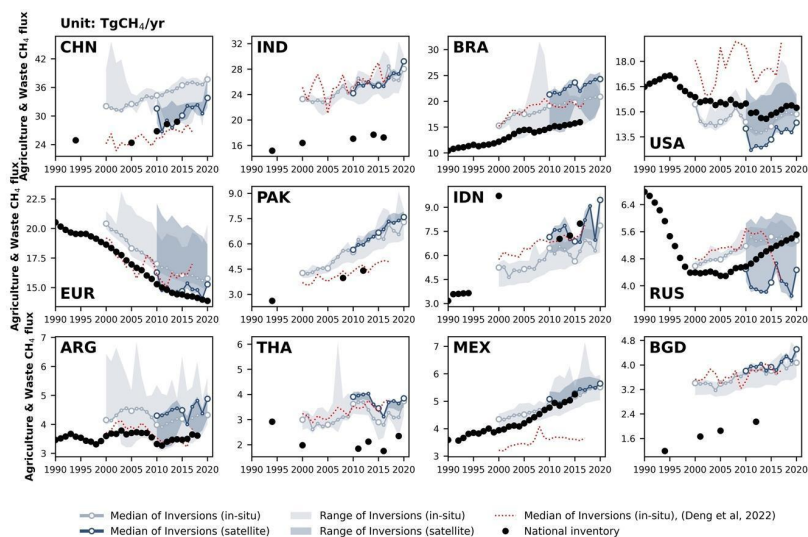
删除了:  $\pm 0.1$

删除了: 65

删除了: 57

'47 and satellite inversions during 2010-2020. However, in MEX, the in-situ inversion was 50% lower than NGHGs in the 2000s  
'48 and showed a sudden large increase in 2010.

'49 **4.3 Agriculture and waste CH<sub>4</sub> emissions**



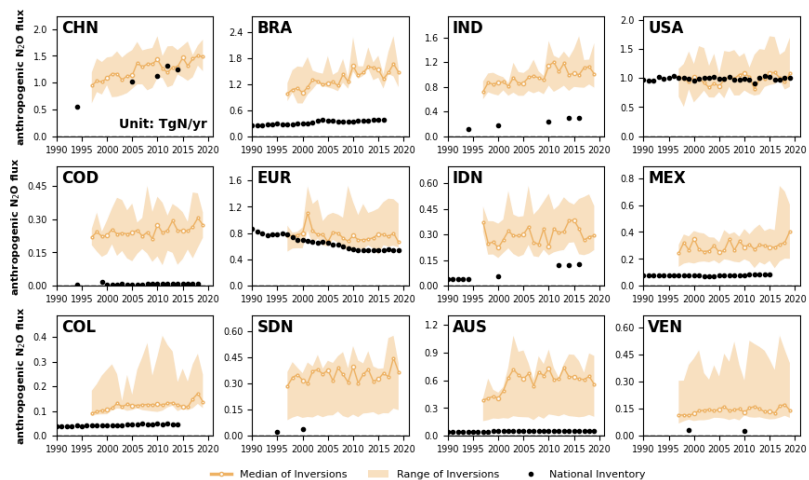
'50  
'51 **Figure 6.** CH<sub>4</sub> emissions from agriculture and waste for the 12 largest emitters in this sector, China (CHN), India (IND), Brazil  
'52 (BRA), United States (USA), European Union (EUR), Pakistan (PAK), Indonesia (IDN), Russia (RUS), Argentina (ARG), Thailand  
'53 (THA), Mexico (MEX), and Bangladesh (BGD). The black dots denote the reported estimates from NGHGs. Other lines, colors, and  
'54 symbols as Fig 4.

'55  
'56 **Fig 6** presents CH<sub>4</sub> emissions of the Agriculture and Waste sector for the top 12 emitters of this sector. In all countries except  
'57 for the United States (USA) and Russia (RUS), the values reported by NGHGs are systematically lower than the inversion  
'58 results. The results from the previous ensemble of in-situ inversions (red dotted line) are consistent with those of the inversions  
'59 used in this study except in the USA where previous inversions are 3.2 TgCH<sub>4</sub>/yr higher, in RUS where they show a drop after  
'60 2015 although they remain in the range from the new satellite and in-situ inversions, and in Mexico (MEX) where they are  
'61 systematically lower by 1.6 TgCH<sub>4</sub>/yr.

'62 In China (CHN), the most recent NGHGI reports in 2012 and 2014 estimate agriculture and waste emissions at 28 Tg CH<sub>4</sub>/yr,  
'63 which is close to satellite inversions (28 ± 1 TgCH<sub>4</sub>/yr) but 22.4% lower than the median in-situ inversions (35 ± 1 TgCH<sub>4</sub>/yr)  
'64 and closer to their minimum value. The trend in agricultural and waste emissions is consistent between inversions and NGHGI  
'65 for CHN. In India (IND), inversions consistently show higher emissions than NGHGI by approximately 50% and indicate an  
'66 increasing trend during 2000-2020, whereas the NGHGI last communication being for 2016, it does not allow us to give a  
'67 recent trend. According to the national inventory of IND, enteric fermentation is the primary source of CH<sub>4</sub> emissions in the  
'68 agriculture and waste sector, contributing 61% of emissions, with rice cultivation accounting for 20% and waste contributing  
'69 16%. A similar pattern is observed in Bangladesh (BGD), where agricultural emissions are dominated by rice production (48%  
'70 in 2012) and enteric fermentation (42% in 2012). Satellite and in-situ inversions estimate emissions in BGD are nearly double  
'71 than those reported by NGHGI during 2001 and 2012, the last communication. The significant discrepancies between  
'72 inversions and NGHGI in IND and BGD may be attributed to potential underestimation of livestock or waste CH<sub>4</sub> emissions  
'73 by NGHGI. NGHGI utilized the Tier 1 method and associated emission factors from the 2006 IPCC Guidelines for National  
'74 Greenhouse Gas Inventories (IPCC, 2006). However, a recent study (Chang et al., 2021) found that estimates using revised  
'75 Tier 1 or Tier 2 methods from the 2019 Refinement to the 2006 IPCC Guidelines for National Greenhouse Gas Inventories  
'76 (IPCC, 2019) give livestock emissions 48%-60% and 42%-61% higher for IND and BGD by 2010, respectively, compared to  
'77 Tier 1 IPCC (2006) methods, which would bring bottom up emissions closer to inversions. In Brazil (BRA), both satellite and  
'78 in-situ inversions consistently estimate larger emissions than the NGHGI by 34% and 29%, respectively, and show a  
'79 consistent increasing trend over their study periods. In the USA, the medians of satellite and in-situ inversions are slightly  
'80 lower than those of NGHGI, but they exhibit a similar trend throughout the study period. The trend of inversions is comparable  
'81 to the one of the NGHGI in BRA during their period of overlap, although there is no NGHGI communication later than 2016.  
'82 In Argentina (ARG), Pakistan (PAK) and Thailand (THA), the medians of in-situ inversions show good consistency with  
'83 satellite inversion results. Nevertheless, in-situ inversion emissions in the 2010s are, on average, 47% higher in PAK, 20%  
'84 higher in ARG, and 64% higher in THA compared to the NGHGI reports. In European Union (EUR), emissions from  
'85 agriculture and waste were reported to have significantly decreased over time in the NGHGI data, mainly from solid waste  
'86 disposal (Petrescu et al., 2021), a trend that is captured by inversions and is close to the one of the NGHGI over the study  
'87 period. In contrast, emissions from agriculture and waste in RUS are reported to have a positive trend after 2010 by the NGHGI,  
'88 with in-situ inversions producing a consistent trend from 2000 to 2014 but a sharp decrease thereafter, while satellite inversions  
'89 are producing stable emissions, albeit lower than the NGHGI and in-situ inversions after 2010.

删除了: 0.5

'91 **5 Results for anthropogenic N<sub>2</sub>O emissions**



'92  
'93 **Figure 7. Anthropogenic N<sub>2</sub>O fluxes of the top 12 emitters: China (CHN), Brazil (BRA), India (IND), United States (USA),**  
'94 **Democratic Republic of the Congo (COD), European Union (EUA), Indonesia (IDN), Mexico (MEX), Colombia (COL), Sudan (SDN),**  
'95 **Australia (AUS), and Venezuela (VEN).** The black dots denote the anthropogenic emissions from the UNFCCC national greenhouse gas  
'96 inventories. The thick orange lines and the light orange areas denote the median and the maximum-minimum ranges of anthropogenic fluxes  
'97 respectively among all N<sub>2</sub>O inversions. We restricted our analysis to data starting from 1997 because it was the year when data from the all  
'98 four inversion models are available.

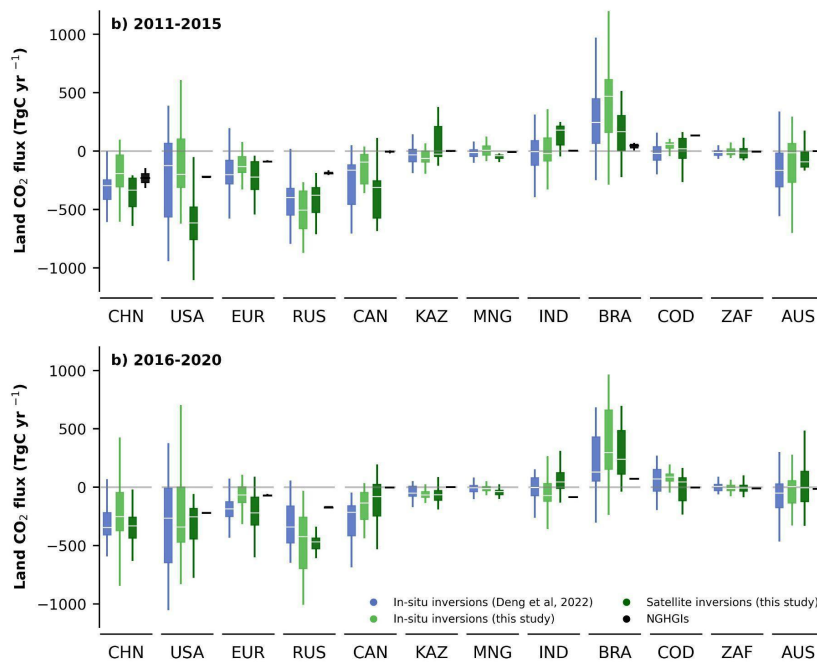
'99  
'00 We present the 12 countries/regions with the largest anthropogenic N<sub>2</sub>O emissions in the world (**Fig 7**), which in total  
'01 contribute approximately 55% of global anthropogenic N<sub>2</sub>O emissions. The estimates from both NGHGs and inversions in  
'02 China (CHN), United States (USA), and European Union (EUR) demonstrate a relatively close match between NGHGs and  
'03 inversions (in-situ only). These three large emitting countries/regions exhibit different trends in their anthropogenic N<sub>2</sub>O  
'04 emissions. In CHN, both NGHGs and inversions indicate an increasing trend in anthropogenic N<sub>2</sub>O emissions. In the USA,  
'05 anthropogenic N<sub>2</sub>O emissions seem to have reached a state of relative stability, with NGHGs and inversion results showing  
'06 similar mean values and lack of trends. In EUR, both NGHGs and inversions show a declining trend in anthropogenic N<sub>2</sub>O  
'07 emissions, but from 2010 to 2020, the NGHGs estimates are lower (20%) than the median values derived from inversion  
'08 models, that is, the negative trend from inversions is less pronounced than the one of NGHGs. Most other selected countries  
'09 display higher anthropogenic N<sub>2</sub>O emissions from inversions than from NGHGs (i.e., Brazil (BRA), India (IND), Democratic

10 Republic of the Congo (COD), Indonesia (IDN), Mexico (MEX), Colombia (COL), Sudan (SDN), Venezuela (VEN)). These  
11 discrepancies in anthropogenic N<sub>2</sub>O emissions are possibly attributable to factors that have been analyzed in our previous study  
12 (Deng et al., 2022). Firstly, nearly all these non-Annex 1 countries utilize Tier 1 emission factors (EFs), which may  
13 underestimate emissions when soil and climate dependence are taken into account (Cui et al., 2021). This has been noted in  
14 previous studies (Philibert et al., 2013; Shcherbak et al., 2014; Wang et al., 2020). Furthermore, the observed concave response  
15 of cropland soil emissions as a function of added N fertilizers may also contribute to underestimated emissions in NGHGs, as  
16 the relationship is non-linear and higher than the linear relation used by NGHGs in Tier 1 approaches (Zhou et al., 2015). In  
17 an improved reporting framework, EFs should also account for both natural and anthropogenic components, as they cannot be  
18 distinguished through field measurements, from which EFs are derived. However, in practice, EFs are mostly based on  
19 measurements made in temperate climates and soils from established croplands with few "background" emissions.  
20 Consequently, there could be a systematic underestimation of default IPCC EFs from tropical climates and for recently  
21 established agricultural lands, for which the IPCC EFs also have a huge uncertainty of up to ±75%–100%. Another factor that  
22 might contribute to the discrepancy is the omission of emissions from reactive nitrogen contained in organic fertilizers  
23 (manure), for which NGHGs do not provide specific details for non-Annex 1 reports. Lastly, anthropogenic indirect emissions  
24 (AIEs) from atmospheric nitrogen deposition and leaching of human-induced nitrogen additions to aquifers and inland waters  
25 are reported by Annex 1 countries using simple emission factors, but non-Annex 1 countries do not consistently report AIE.  
26 However, in Australia (AUS), the gap between inversions and NGHGs has even expanded compared to our previous study.  
27 We do acknowledge that the density of the N<sub>2</sub>O in-situ network in tropical countries and around AUS is so low that inversions  
28 most likely are attracted to their priors. The use of a lower prior could thus also be consistent with scarce atmospheric  
29 observations, and we have only a low confidence on N<sub>2</sub>O inversion results for tropical countries and AUS.

删除了: is

31 **6 Discussion**

32 **6.1 Comparing net land CO<sub>2</sub> flux estimates from different inversion model ensembles**



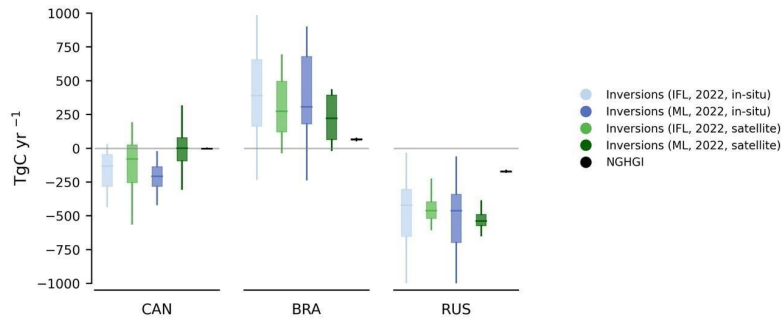
33 **Figure 8.** Net CO<sub>2</sub> land fluxes during the period of a) 2011-2015; and b) 2016-2020 in China (CHN), United States (USA), European  
34 Union (EUR), Russia (RUS), Canada (CAN), Kazakhstan (KAZ), Mongolia (MNG), India (IND), Brazil (BRA), Democratic Republic  
35 of the Congo (COD), South Africa (ZAF), and Australia (AUS). Blue boxes denote the in-situ inversion results from Deng et al. (2022)  
36 processed from Global Carbon Budget 2020 (Friedlingstein et al., 2020). Light green boxes denote the in-situ inversion results processed in  
37 this study, while dark green boxes denote the satellite inversion results. Black boxes denote the NGHGs reported values. The white lines in  
38



39 the boxes denote the medians of the land CO<sub>2</sub> fluxes. Note that the inversion results here have been adjusted by the lateral flux before the  
40 comparison. Additionally, we extend the comparison with national land use change emissions from global bookkeeping models in Fig S4.  
41 In this section, we compare four different estimates of land CO<sub>2</sub> fluxes during the period 2010-2020 (**Fig 8**), including: 1)  
42 medians of in-situ inversion results from our previous study (Deng et al., 2022), 2) medians of in-situ and 3) satellite-based  
43 inversion results processed in this study based on the Global Carbon Budget 2022 (Friedlingstein et al., 2022), and 4) NGHGs.  
44 This enables a comparison of the median and range of our in-situ inversion results (n=5) with those from previous study (n=6),  
45 and assesses the performance differences between satellite-based (n=4) and in-situ inversion models. To ensure a fair  
46 comparison and avoid anomalies in the satellite-based inversion results during 2010-2015 when some of these inversions used  
47 GOSAT after 2010 and then OCO-2 after 2015, we separate the analysis into two periods: 2011-2015 and 2016-2020.  
48 The variations of yearly land CO<sub>2</sub> fluxes span a comparable range between the current and previous in-situ inversion ensembles,  
49 indicating that consistency of the inversion results, but the uncertainty within the new in-situ inversion ensemble was not  
50 improved. However, examining the median values, results from the new in-situ inversion ensemble may be closer to NGHGs  
51 in most countries (such as China (CHN), United States (USA), European Union (EUR), Canada (CAN), Kazakhstan (KAZ),  
52 India (IND)). This suggests that the new in-situ inversion ensemble used in this study has partially narrowed down the gaps  
53 between inversion results and NGHGs compared to the previous one. However, in Russia (RUS) and Brazil (BRA), the  
54 difference between the median of in-situ inversion ensembles and NGHGs has enlarged. For example, in RUS, median the  
55 new in-situ inversion ensemble indicate a larger carbon sink than those from Deng et al. (2022), while the difference between  
56 median of in-situ inversions and NGHGs increases 51% during 2011-2015 (from 208 TgC/yr to 314 TgC/yr) and 49% during  
57 2016-2020 (from 168 TgC/yr to 249 TgC/yr). Conversely, in BRA, median of the new in-situ inversion ensemble indicate a  
58 larger carbon source, while the difference increases over 100% during 2011-2015 (from 200 TgC/yr to 423 TgC/yr) and nearly  
59 300% during 2016-2020 (from 56 TgC/yr to 223 TgC/yr).  
60 As for the inversion ensemble used in this study, in most countries, the variations of yearly land CO<sub>2</sub> fluxes also span a similar  
61 range between satellite-based inversion ensemble and in-situ inversion ensemble. However, in the cases of USA, RUS, CHN  
62 and BRA, the spread of satellite-based inversion results are narrower than those of in-situ inversion results, indicating a better  
63 consistency among available satellite-based inversion models, at least when similar satellite data are assimilated. In addition,  
64 in most cases, smaller differences were found between the median of inversion results and the NGHGs. For countries with  
65 dense surface monitoring networks such as in the USA and EUR, the satellite-based inversion results show good agreement  
66 in-situ inversion results. However, for countries with sparse station coverage like Kazakhstan (KAZ) and Mongolia (MNG),  
67 satellite-based inversion results could provide more reliable estimates due to more extensive spatial sampling from satellites,  
68 although the medians of satellite-based inversion results indicate larger carbon sinks and larger differences compared with  
69 NGHGs (than for in-situ inversion results). In USA and CAN, the difference during 2011-2015 (only GOSAT period) between  
70 in-situ and satellite-based inversion ensembles is larger than that during 2016-2020 (OCO-2 period). This can be attributed to  
71 the use of different satellite data during these periods and different numbers of ensemble members. Before 2015, only GOSAT

72 was available, and only 2 out of 4 systems. The inversion of OCO-2 data starting in 2014 resulted in a better alignment among  
73 OCO-2 ACOS v10 inversions, indicating the in-situ and satellite evaluations were similar (Byrne et al., 2023).

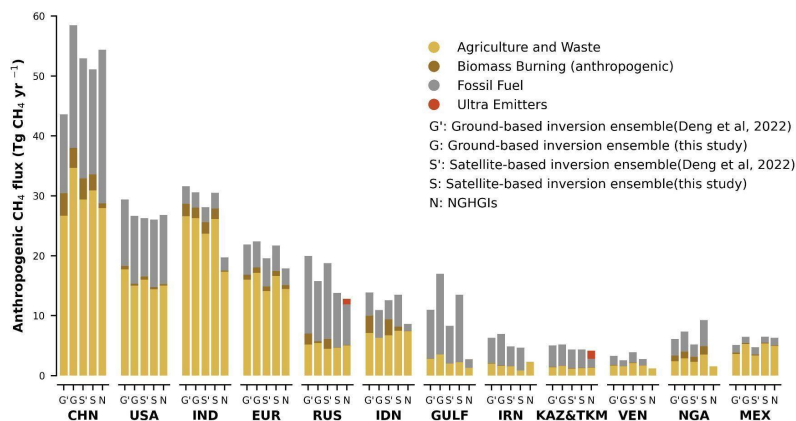
## 74 6.2 Adjustment of the national managed land masks to separate the net land CO<sub>2</sub> flux estimates



75 **Figure 9. Net CO<sub>2</sub> land fluxes during the period of 2015-2020 in Canada (CAN), Brazil (BRA), and Russia (RUS).** 'IFL' stands for  
76 using the intact forest landscape data as a mask for non-managed land to extract land CO<sub>2</sub> flux from managed land and 'ML' indicates the  
77 adjusted mask used by Grassi et al. (2023) to extract land CO<sub>2</sub> flux from managed land. The 'in-situ' stands for inversion results using in-  
78 situ observations, and 'satellite' represents inversions using satellite observations. Note that the inversion results here have been adjusted by  
79 the lateral flux before the comparison.  
80

81 Following the method proposed by Grassi et al. (2023), we updated in this study the managed land mask for Canada (CAN)  
82 and Brazil (BRA) by using maps of managed land derived from NGHGI, and for Russia (RUS) by adjusting tree-cover  
83 threshold in the tree cover map from Hansen et al. (2013) to match the average area of managed land per Oblast (province)  
84 that is used for the NGHGIs. Thus, the new mask is now more consistent with the definition of managed land in the NGHGIs  
85 for these three countries, so that can further analyze the impacts of different definitions of managed land masks to separate the  
86 managed land CO<sub>2</sub> fluxes in inversions (Fig 9). Generally, in Russia (RUS) and Canada (CAN), the managed land CO<sub>2</sub> fluxes  
87 extracted from the new mask are closer to NGHGIs than those separated by the previous mask used by Deng et al. 2022. In  
88 addition, in Brazil (BRA), adjusting the national managed land mask resulted in greater land carbon emissions, increasing the  
89 gap with NGHGIs. However, the improvement of the managed land mask in this study is still not able to explain all the existing  
90 discrepancy between inversion estimates and NGHGIs, in which the sources and reasons for these differences and uncertainties  
91 still need further analysis. We also observe in Fig. 9 that the impact of our new managed land mask compared to the previous  
92 one, is qualitatively similar whether it is applied to in-situ inversions or satellite inversions gridded flux fields.

93 **6.3 Comparison of anthropogenic CH<sub>4</sub> emissions with Deng et al 2022**



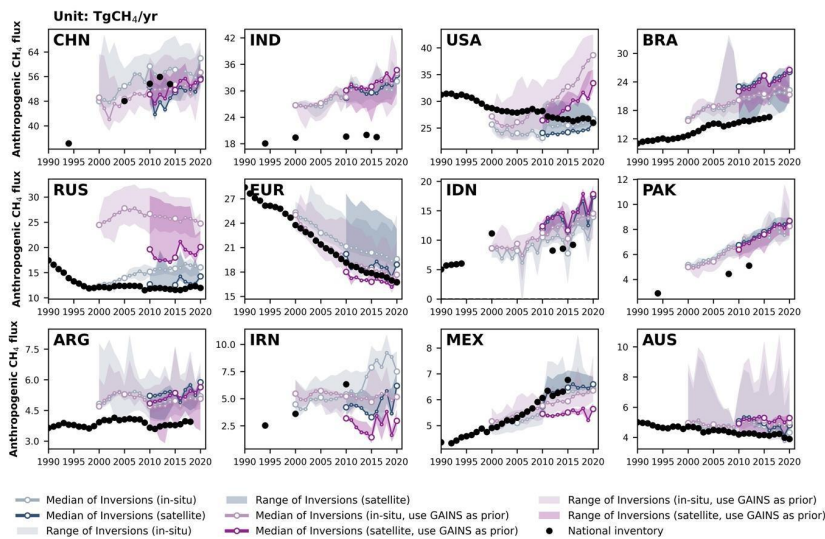
94  
95 **Figure 10. Annual average of anthropogenic CH<sub>4</sub> emissions from in-situ (G) and satellite (S) inversions and national greenhouse gas**  
96 **inventories (N) during the period of 2010-2020. G' and S' denote the anthropogenic CH<sub>4</sub> flux from the in-situ and satellite inversion**  
97 **ensembles in the previous study (Deng et al., 2022) respectively, while G and S denote the fluxes from the in-situ and satellite inversion**  
98 **ensembles used in this study. N denotes the estimates from NGHGs. Grey, yellow, and brown bars represent the CH<sub>4</sub> fluxes from the sectors**  
99 **of fossil fuel combustion, agriculture and waste, and biomass burning respectively. On top of NGHGI emissions, emissions from ultra-**  
00 **emitters (red) are added to NGHGI estimates (diagnosed from S5P-TROPOMI measurements for the period 2019–2020; Lauvaux et al.,**  
01 **2022).**

02 In our previous study, we found that satellite inversion models appear to have a better agreement with NGHGs than in-situ  
03 stations based inversion models, and on the other hand, that differences between inversion models and NGHGs in large oil-  
04 and gas-producing countries suggest an underestimation of national reports, possibly due to the omission of ultra-emitting  
05 sources by NGHGs. With the new inversion ensemble in this study, we confirm those results (Fig 10). In countries such as  
06 China (CHN), India (IND), and Russia (RUS), the updated inversion model set provides estimates that are closer to NGHGs,  
07 but differences still exist, and the reasons for these differences are not the same. For example, differences in anthropogenic  
08 methane emissions in IND are mainly due to differences in agricultural and waste methane flux with the new inversion  
09 ensemble used in this study. In RUS, the updated inversion ensemble shows lower fossil fuel emissions, reducing the  
10 differences with NGHGs for this sector, but higher agricultural and waste emissions than in Deng et al. (2022). Nevertheless,  
11 the updated fossil fuel emission flux is still higher than the NGHGs estimate for RUS. The remaining differences may be  
12 attributed to ultra-emitting sources or underestimated emission factors for some components of the oil and gas extraction and  
13 distribution industry in RUS. Conversely, in GULF (GULF = Saudi Arabia + Iraq + Kuwait + Oman + United Arab Emirates

删除了: agreement

15 + Bahrain + Qatar), the new inversion model ensemble consistently reflects higher fossil fuel emission fluxes than NGHGs  
 16 like in our previous study, and expands the difference in estimates of artificial methane flux between inversion models and  
 17 NGHGs, possibly indicating more methane leakage.

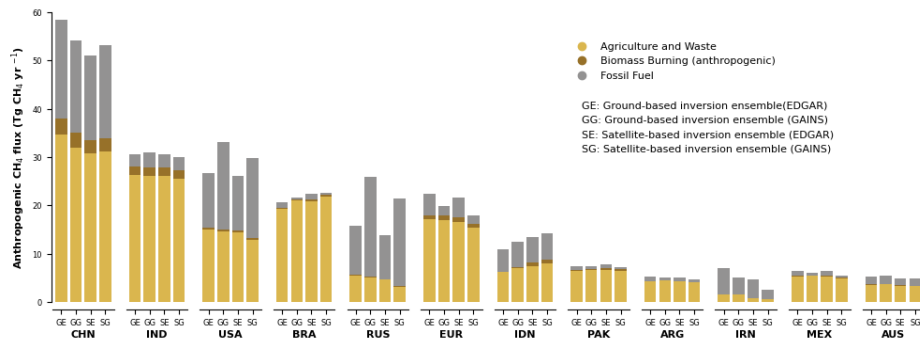
18 **6.4 Influence of the prior used in CH<sub>4</sub> inversions**



19 **Figure 11. Total anthropogenic CH<sub>4</sub> fluxes for the 12 top emitters: China (CHN), India (IND), United States (USA), Brazil (BRA),**  
 20 **Russia (RUS), European Union (EUR), Indonesia (IDN), Pakistan (PAK), Argentina (ARG), Iran (IRN), Mexico (MEX), and**  
 21 **Australia (AUS).** The black dots denote the reported values from NGHGs. The light blue lines/areas denote the median and maximum-  
 22 minimum ranges of in-situ CH<sub>4</sub> inversions based on EDGARv6.0 as the prior and the dark blue ones of satellite inversions, respectively.  
 23 The light purple lines/areas denote the median and maximum-minimum ranges of in-situ CH<sub>4</sub> inversions based on GAINS (Höglund-Isaksson  
 24 et al., 2020) as the prior and the dark purple ones of satellite inversions, respectively.  
 25  
 26

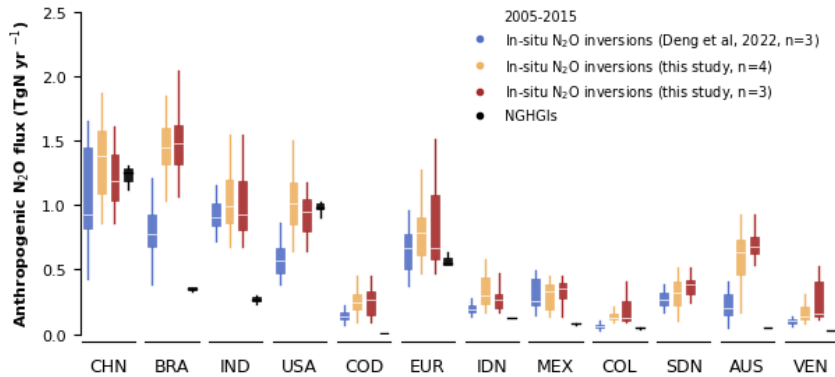
27 The use of different priors can also influence the inversion results of the data. **Fig 11** presents the sets of inversion results using  
 28 EDGAR (blue) and GAINS (purple) as priors. In most countries, the median values of the two inversion result sets are similar.  
 29 However, in countries such as Russia (RUS), United States (USA), Iran (IRN), Mexico (MEX), significant differences are  
 30 observed between the two inversion result sets, which may primarily stem from the differences in the inversion results for  
 31 fossil CH<sub>4</sub> emissions (**Fig 12**). In RUS and USA, the inversion results using GAINS as priors are consistently higher than those

132 using EDGAR as priors. In RUS, the satellite inversion results using GAINS as priors are higher by 45% during 2010-2020,  
 133 and the ground-based inversion results are higher by 75% during 2000-2020. In the case of the USA, the inversion results  
 134 using GAINS as priors exhibit a completely different trend compared to the ones obtained using NGHGs and EDGAR as  
 135 priors. The inversion results using GAINS as priors, both from satellite and ground-based measurements, show a rapid growth  
 136 trend by increasing 24% from 2010 to 2020. In IRN and MEX, the inversion results using GAINS as priors are lower than  
 137 those using EDGAR as priors. For IRN, the differences between satellite inversion results using different priors are not  
 138 significant, and the trends are similar. However, the ground-based inversion results are very close between 2000-2013, but  
 139 after 2013, a steep increase is observed in the ground-based inversion results using GAINS as priors. On the other hand, in  
 140 MEX, the ground-based inversion results are similar, but the satellite inversion results using GAINS as priors are relatively  
 141 lower by 14% averagely. Such discrepancies may arise from differences in inventory methodologies and the resulting  
 142 estimations. As shown in Supplementary Figure S1 in Tibrewal et al. (2024), similar discrepancies were found between the  
 143 two inventories in these countries, which reports a higher estimation from GAINS in RUS and USA compared to EDGAR  
 144 during 2011-2020, and a lower estimation in IRN. As noted in Tibrewal et al. (2024), EDGAR is based on various versions of  
 145 National Inventory Reports (NIR) that utilize different combinations of emission factors from the IPCC, while GAINS employs  
 146 an independent estimation approach. This highlights the critical role of prior data selection in determining the accuracy of CH<sub>4</sub>  
 147 emission estimates.



148 Fig. 12. Annual average of anthropogenic CH<sub>4</sub> emissions from in-situ and satellite inversions based on two different priors  
 149 during the period of 2010-2020. GE and SE denote the anthropogenic CH<sub>4</sub> flux from the in-situ and satellite inversion  
 150 ensembles based on EDGARv6.0 as the prior, while GG and SG represent the in-situ and satellite CH<sub>4</sub> inversions based on  
 151 GAINS as the prior.  
 152

53 **6.5 Comparing anthropogenic N<sub>2</sub>O flux with the previous study**



54 **Figure 13. Anthropogenic N<sub>2</sub>O fluxes during the period of 2005-2015 in China (CHN), Brazil (BRA), India (IND), United States**  
 55 **(USA), Democratic Republic of the Congo (COD), European Union (EUR), Indonesia (IDN), Mexico (MEX), Colombia (COL), SDN**  
 56 **(Sudan), Australia (AUS), and Venezuela (VEN).** Blue boxes denote the in-situ inversion results from Deng et al. 2022 processed from  
 57 Global Carbon Budget 2020 (Friedlingstein et al., 2020). Dark yellow boxes denote the inversion results processed in this study. Black boxes  
 58 denote the NGHGIs reported values.  
 59

60  
 61 The updated N<sub>2</sub>O inversion results show systematically higher anthropogenic emissions than the previous N<sub>2</sub>O inversion results  
 62 (Deng et al, 2022), resulting in larger discrepancies between N<sub>2</sub>O inversion results and NGHGIs in most countries in Fig 13,  
 63 Countries such as Brazil (BRA), Democratic Republic of the Congo (COD), Indonesia (IDN), Colombia (COL), Sudan (SDN),  
 64 Australia (AUS), and Venezuela (VEN) exhibit significant differences. These discrepancies may be attributed to the use of  
 65 lower IPCC default emission factors in the national inventories of these tropical countries, leading to lower NGHGI results.  
 66 The IPCC default emission factors are derived from measurements primarily conducted in temperate regions of the Northern  
 67 Hemisphere (e.g., Europe and the United States (USA)), which explains the better alignment of inversion results with  
 68 inventories in those regions. Notably, , in the case of the USA, the median of the updated N<sub>2</sub>O inversion results is very close  
 69 to NGHGIs. The median of the N<sub>2</sub>O inversion results from Deng et al. (2022) was 42% lower than the NGHGIs between 2005  
 70 and 2015, whereas the median of the updated inversion models is only 4% lower. This demonstrates improved consistency in  
 71 the updated inversion system results for the USA. Additionally, in countries such as India (IND), IDN, COL, COD, Sudan  
 72 (SDN), and VEN, our N<sub>2</sub>O inversion results have a larger distribution compared to the previous study, indicating that the new  
 73 N<sub>2</sub>O inversion ensemble (n=4) has less consistency in these countries compared to the previous ensemble (n=3).

74 **Conclusions**

75 This study reconciles the gap between atmospheric inversions and UNFCCC NGHGs for each of the three greenhouse gases,  
76 based on the post-processing framework we proposed in our previous study (Deng et al., 2022). We update inversion results  
77 and NGHGs datasets to present the most-up-to-date discrepancies between these two estimates. For CO<sub>2</sub>, we updated the  
78 inversion results up to 2021, added a new inversion ensemble including inversions based on satellite observations, and applied  
79 a new mask of national managed land based on NGHGI reports in Russia, Brazil and Canada. For CH<sub>4</sub>, we compared NGHGs  
80 and CH<sub>4</sub> inversion results up to 2020 by splitting the anthropogenic fluxes from inversions by aggregating prior estimates from  
81 each sector or by removing fluxes of natural processes and discussed the uncertainties by using different priors in CH<sub>4</sub>  
82 inversions. For N<sub>2</sub>O, we updated the inversion results up to 2019 and included the MIROC4-ACTM N<sub>2</sub>O inversion, also  
83 separated the fluxes from managed land by using the same method on CO<sub>2</sub>.

84 In the case of CO<sub>2</sub>, we updated the managed land mask for Canada, Brazil, and Russia based on maps derived from NGHGs  
85 and adjusted tree-cover thresholds. The analysis of different managed land mask definitions shows that the new mask, which  
86 is more consistent with the definition of managed land in the NGHGs for these countries, improves the agreement between  
87 managed land CO<sub>2</sub> fluxes and NGHGs in Russia and Canada. However, in Brazil, the new mask increases the gap between  
88 the estimated land carbon emissions and NGHGs. Further analysis is needed to understand the sources and reasons for  
89 discrepancies and uncertainties between inversion estimates and NGHGs. Thus, we still recommend that countries should  
90 report their managed land in a spatially explicit manner to enable a better evaluation of national emission reports using  
91 inversions (and other observation-based approaches), and countries should also follow the recommendations of the IPCC 2006  
92 Guidelines encouraging countries to use atmospheric data as an independent check on their national reports (IPCC 2006, 2019).  
93 Three additional satellite-based inversion results have been introduced for comparison with the in-situ inversion results and  
94 NGHGs. In some countries, the satellite-based inversions demonstrate better consistency with NGHGs compared to the in-  
95 situ inversion models.

96 For CH<sub>4</sub>, despite the large spread of inversions, both in-situ and GOSAT inversions show systematic differences with NGHGs.  
97 We also found that Kazakhstan and Turkmenistan in Central Asia and the Gulf countries in the Middle East, characterized by  
98 oil- and gas-producing industries, report much less CH<sub>4</sub> emissions than atmospheric inversions estimates. While in this region,  
99 there are few ground stations, and inversions depend on their prior fluxes, the fact that GOSAT and in-situ based inversions  
00 point to NGHGI emissions being underestimated suggests areas for future research to constrain the emissions of these countries.  
01 We recommend here to develop regional campaigns (such as those performed in Alvarez et al. (2018)), to refine emission  
02 factors, and to track regional oil, gas and coal basins emissions and ultra-emitter site-level emissions using new tools (such as  
03 moderate and high-resolution satellite imagery).

04 For N<sub>2</sub>O, the prevalence of large tropical natural sources, being outside the responsibility of countries if they are located on  
05 unmanaged lands, has been overlooked before. For example, nearly half of the forests in Brazil are unmanaged according to  
06 its national inventory report. We did not solve this problem, but highlighted it and proposed a new method to remove natural

007 emissions from inversion total emissions. As many non-Annex I countries, which will have to produce inventories for the  
008 global stocktake are tropical countries with a very active nitrogen cycle and large natural N<sub>2</sub>O emissions, a decoupling will  
009 exist between targeted emissions reductions and the observed growth rate of N<sub>2</sub>O: it may hamper the eventual effectiveness of  
010 mitigation policies, that are directly reflected in the UNFCCC NGHGs reports, especially for this greenhouse gas. It is fair to  
011 say that the uncertainty from the spread of different inversions is large enough that inversions cannot ‘falsify’ N<sub>2</sub>O NGHGs  
012 in most instances. Nevertheless, for CH<sub>4</sub> in countries around the Persian Gulf and Central Asia, and to some extent in Russia,  
013 and for N<sub>2</sub>O in tropical countries, Mexico and Australia, we found that NGHGs emissions are significantly lower than  
014 inversions, which suggests that activity data or emission factors may need to be re-evaluated. Despite their large spread,  
015 inversions have the advantage of providing fluxes that are consistent with the accurately observed growth rates of each  
016 greenhouse gas in the atmosphere. The uncertainty of inversions is mainly a systematic bias due to internal settings or to the  
017 choice of a transport model. It does not mean that inversions cannot be used for monitoring interannual variability and trends  
018 of fluxes, in response to mitigation efforts, since most of their bias should have a small temporal component.

019 The study of global inversions at the country scale rather than at the traditional subcontinent scale (e.g. the “Transcom3 regions”  
020 of Gurney et al. (2002)) obviously pushes inversions close to the limit of their domain of validity, even in the case of large  
021 countries. The densification of observation networks and systems, especially from space, increases the observational  
022 information available at all spatial scales and gradually makes it possible to study smaller countries and reduce uncertainties  
023 of inversion results. This densification must be accompanied by a corresponding increase in the horizontal resolution of  
024 inversion systems (both the transport model and the control vector to be optimized). Note that the spatial resolution of most  
025 inverse models such as those contributing to the global carbon/methane/nitrous oxide budget is larger than 1 degree (see Table  
026 A4 in Friedlingstein et al. (2022), Table S6 in Saunio et al. (2020), and Table 1 in Tian et al. (2023)). They will likely soon  
027 have to go below one degree on a global scale to remain competitive for this type of study, despite the high computational  
028 challenge posed by the atmospheric inversion of long-lived tracers.

#### 029 **Data availability**

030 Processed GHG (CO<sub>2</sub>, CH<sub>4</sub>, and N<sub>2</sub>O) data from inverse models and UNFCCC NGHGs are available at  
031 <https://doi.org/10.5281/zenodo.13887128> (Deng et al., 2024).

032 This dataset contains 5 data files:

- 033 - The file *Inversions\_CO2\_v2022.csv* includes the NEE CO<sub>2</sub> flux from managed lands for the nine CO<sub>2</sub> inverse models.  
034 It includes 8 fields: years (from 1960 to 2021), country, value (unit: TgC/yr), sector ("land": without the adjustment  
035 of lateral C flux; "land\_cor": with later C flux adjustment), source, gas, observation ("in-situ": in-situ-based; "satellite":  
036 satellite-based), version ("CO2\_ML\_v2022" only).
- 037 - The file *Inversions\_CH4\_v2022.csv* includes CH<sub>4</sub> flux from anthropogenic sources for the six CH<sub>4</sub> inverse models.  
038 It includes 8 fields: years (from 2000 to 2020), country, value (unit: TgCH<sub>4</sub>/yr), sector ("agrw": agriculture and waste;



139 "fos": fossil fuel; "ant": anthropogenic=agrw+fos), source, gas, observation ("in-situ": in-situ-based; "satellite":  
140 satellite-based), version ("CH4\_2022\_V1": use EDGAR as priors; "CH4\_2022\_V2": use GAINS as priors).  
141 - The file *Inversions\_N2O\_v2022.csv* includes the anthropogenic N2O flux from managed lands for the four N2O  
142 inverse models. It includes 8 fields: years (from 1995 to 2020), country, value (unit: TgN2O/yr), sector ("ant" only,  
143 for anthropogenic), source, gas, observation ("in-situ" only, for in-situ-based), version ("N2O\_ML\_v2022" only).  
144 - The file *lateral\_CO2\_v2022.csv* includes the national lateral C flux from river and trade.  
145 - The file *NGHGs\_v2022.csv* includes the national inventory data collected from UNFCCC NGHGs (unit: Gg/yr)

#### 146 **Author contribution**

147 PC, FC, MS, RLT, and ZD designed and coordinated the study. PC, MS, RLT, and FC designed the framework of atmosphere  
148 inversion data processing. ZD, PC, LH, MS, RLT, and FC performed the post-processing and analysis and wrote the paper.  
149 ZD, LH, and TW compiled the national greenhouse gas inventories. MS, RLT, HT, and FC gathered the global atmosphere  
150 inversion datasets of CO2, CH4, and N2O. GG contributed the managed land mask of Brazil and Canada. FC processed the  
151 atmosphere inversion data with masks of managed lands and country boundaries. AT, SM, RJ, YN, BZ, JT, DB and AS  
152 contribute the unpublished CH4 inversion data. All authors contributed to the full text.

#### 153 **Competing interests**

154 At least one of the (co-)authors is a member of the editorial board of Earth System Science Data.

#### 155 **Acknowledgements**

156 The authors are very grateful to the atmosphere inversion model developers Chris Wilson, Christian Rödenbeck, Kelley Wells,  
157 Liesbeth Florentie, Naveen Chandra, Peter Bergamaschi, Prabir Patra, and Yi Yin for the availability of their global CO2, CH4,  
158 and N2O inversion data and acknowledge many other data providers (measurements, models, inventories, atmospheric  
159 inversions, hybrid products, etc.) that are directly or indirectly used in this synthesis. The PyVAR-CAMS N2O modelling  
160 results were funded through the Copernicus Atmospheric Monitoring Service, implemented by ECMWF on behalf of the  
161 European Commission and were generated using computing resources from LSCE. Rona Thompson would also like to  
162 acknowledge the support of Frederic Chevallier in providing the PyVAR-CAMS N2O inversion results.

#### 163 **References**

164 Aragão, L. E. O. C., Anderson, L. O., Fonseca, M. G., Rosan, T. M., Vedovato, L. B., Wagner, F. H., Silva, C. V. J., Silva Junior, C. H. L.,  
165 Arai, E., Aguiar, A. P., Barlow, J., Berenguer, E., Deeter, M. N., Domingues, L. G., Gatti, L., Gloor, M., Malhi, Y., Marengo, J. A.,

166 Miller, J. B., Phillips, O. L., and Saatchi, S.: 21st Century drought-related fires counteract the decline of Amazon deforestation  
167 carbon emissions, *Nat. Commun.*, 9, 536, 2018.

168 Berchet, A., Sollum, E., Thompson, R. L., Pison, I., Thanwerdas, J., Broquet, G., Chevallier, F., Aalto, T., Berchet, A., Bergamaschi, P.,  
169 Brunner, D., Engelen, R., Fortems-Cheiney, A., Gerbig, C., Groot Zwaaftink, C. D., Haussaire, J.-M., Henne, S., Houweling, S.,  
170 Karstens, U., Kutsch, W. L., Lujikx, I. T., Monteil, G., Palmer, P. I., van Peet, J. C. A., Peters, W., Peylin, P., Potier, E., Rödenbeck,  
171 C., Saunois, M., Scholze, M., Tsuruta, A., and Zhao, Y.: The Community Inversion Framework v1.0: a unified system for  
172 atmospheric inversion studies, *Geoscientific Model Development*, 14, 5331–5354, 2021.

173 Byrne, B., Liu, J., Lee, M., Yin, Y., Bowman, K. W., Miyazaki, K., Norton, A. J., Joiner, J., Pollard, D. F., Griffith, D. W. T., Velazco, V.  
174 A., N. M. Deutscher, Jones, N. B., and Paton-Walsh, C.: The carbon cycle of southeast Australia during 2019–2020: Drought, fires,  
175 and subsequent recovery, *AGU Advances*, 2, <https://doi.org/10.1029/2021av000469>, 2021.

176 Byrne, B., Baker, D. F., Basu, S., Bertolacci, M., Bowman, K. W., Carroll, D., Chatterjee, A., Chevallier, F., Ciais, P., Cressie, N., Crisp,  
177 D., Crowell, S., Deng, F., Deng, Z., Deutscher, Nicholas M, Dubey, M. K., Feng, S., García, O. E., Griffith, D. W. T., Herkommer,  
178 B., Hu, L., Jacobson, A. R., Janardanan, R., Jeong, S., Johnson, M. S., Jones, D. B. A., Kivi, R., Liu, J., Liu, Z., Maksyutov, S.,  
179 Miller, J. B., Miller, S. M., Morino, I., Notholt, J., Oda, T., O'Dell, C. W., Oh, Y.-S., Ohyama, H., Patra, P. K., Peiro, H., Petri, C.,  
180 Philip, S., Pollard, D. F., Poulter, B., Remaud, M., Schuh, A., Sha, M. K., Shiomi, K., Strong, K., Sweeney, C., Té, Y., Tian, H.,  
181 Velazco, V. A., Vrekoussis, M., Wameke, T., Worden, J. R., Wunch, D., Yao, Y., Yun, J., Zammit-Mangion, A., and Zeng, N.:  
182 National CO<sub>2</sub> budgets (2015–2020) inferred from atmospheric CO<sub>2</sub> observations in support of the global stocktake, *Earth System  
183 Science Data*, 15, 963–1004, 2023.

184 Chandra, N., Patra, P. K., Bisht, J. S. H., Ito, A., Umezawa, T., Saigusa, N., Morimoto, S., Aoki, S., Janssens-Maenhout, G., Fujita, R.,  
185 Takigawa, M., Watanabe, S., Saitoh, N., and Canadell, J. G.: Emissions from the Oil and Gas Sectors, Coal Mining and Ruminant  
186 Farming Drive Methane Growth over the Past Three Decades, *Journal of the Meteorological Society of Japan. Ser. II*, 99, 309–337,  
187 2021.

188 Chang, J., Ciais, P., Gasser, T., Smith, P., Herrero, M., Havlik, P., Obersteiner, M., Guenet, B., Goll, D. S., Li, W., Naipal, V., Peng, S.,  
189 Qiu, C., Tian, H., Viomy, N., Yue, C., and Zhu, D.: Climate warming from managed grasslands cancels the cooling effect of carbon  
190 sinks in sparsely grazed and natural grasslands, *Nat. Commun.*, 12, 118, 2021.

191 Chevallier, F.: Fluxes of carbon dioxide from managed ecosystems estimated by national inventories compared to atmospheric inverse  
192 modeling, *Geophys. Res. Lett.*, 48, <https://doi.org/10.1029/2021gl093565>, 2021.

193 Chevallier, F., Fisher, M., Peylin, P., Serrar, S., Bousquet, P., Bréon, F.-M., Chédin, A., and Ciais, P.: Inferring CO<sub>2</sub> sources and sinks

994 from satellite observations: Method and application to TOVS data, *J. Geophys. Res.*, 110, <https://doi.org/10.1029/2005jd006390>,  
995 2005.

996 Ciais, P., Yao, Y., Gasser, T., Baccini, A., Wang, Y., Lauerwald, R., Peng, S., Bastos, A., Li, W., Raymond, P. A., Canadell, J. G., Peters,  
997 G. P., Andres, R. J., Chang, J., Yue, C., Dolman, A. J., Haverd, V., Hartmann, J., Laruelle, G., Konings, A. G., King, A. W., Liu, Y.,  
998 Luyssaert, S., Maignan, F., Patra, P. K., Peregon, A., Regnier, P., Pongratz, J., Poulter, B., Shvidenko, A., Valentini, R., Wang, R.,  
999 Broquet, G., Yin, Y., Zscheischler, J., Guenet, B., Goll, D. S., Ballantyne, A.-P., Yang, H., Qiu, C., and Zhu, D.: Empirical estimates  
000 of regional carbon budgets imply reduced global soil heterotrophic respiration, *Natl Sci Rev*, 8, nwaal45, 2021.

001 Cui, X., Zhou, F., Ciais, P., Davidson, E. A., Tubiello, F. N., Niu, X., Ju, X., Canadell, J. G., Bouwman, A. F., Jackson, R. B., Mueller, N.  
002 D., Zheng, X., Kanter, D. R., Tian, H., Adalibekie, W., Bo, Y., Wang, Q., Zhan, X., and Zhu, D.: Global mapping of crop-specific  
003 emission factors highlights hotspots of nitrous oxide mitigation, *Nat Food*, 2, 886–893, 2021.

004 Deng, Z., Ciais, P., Tzompa-Sosa, Z. A., Saunio, M., Qiu, C., Tan, C., Sun, T., Ke, P., Cui, Y., Tanaka, K., Lin, X., Thompson, R. L.,  
005 Tian, H., Yao, Y., Huang, Y., Lauerwald, R., Jain, A. K., Xu, X., Bastos, A., Sitch, S., Palmer, P. I., Lauvaux, T., d'Aspremont, A.,  
006 Giron, C., Benoit, A., Poulter, B., Chang, J., Petrescu, A. M. R., Davis, S. J., Liu, Z., Grassi, G., Albergel, C., Tubiello, F. N.,  
007 Perugini, L., Peters, W., and Chevallier, F.: Comparing national greenhouse gas budgets reported in UNFCCC inventories against  
008 atmospheric inversions, *Earth Syst. Sci. Data*, 14, 1639–1675, 2022.

009 Deng, Z., Ciais, P., Hu, L., Wang, T., Martinez, A., Saunio, M., Thompson, R., and Chevallier, F.: Global greenhouse gas reconciliation  
010 2022, 2024. <https://doi.org/10.5281/zenodo.13887128>

011 [FAO: Trade, FAOSTAT, 2024. available at: https://www.fao.org/faostat/en/#data](https://www.fao.org/faostat/en/#data). FAO, Rome, Italy.

012 Feng, L., Palmer, P. I., Parker, R. J., N. M. Deutscher, Feist, D. G., Kivi, R., Morino, I., and Sussmann, R.: Estimates of European uptake  
013 of CO<sub>2</sub> inferred from GOSAT XCO<sub>2</sub> retrievals: sensitivity to measurement bias inside and outside Europe, *Atmos. Chem. Phys.*, 16,  
014 1289–1302, 2016.

015 Flammini, A., Adzmir, H., Karl, K., and Tubiello, F. N.: Quantifying greenhouse gas emissions from wood fuel use by households, *Earth*  
016 *Syst. Sci. Data*, 15, 2179–2187, <https://doi.org/10.5194/essd-15-2179-2023>, 2023.

017 Friedlingstein, P., O'Sullivan, M., Jones, M. W., Andrew, R. M., Hauck, J., Olsen, A., Peters, G. P., Peters, W., Pongratz, J., Sitch, S., Le  
018 Quéré, C., Canadell, J. G., Ciais, P., Jackson, R. B., Alin, S., Aragão, L. E. O. C., Armeth, A., Arora, V., Bates, N. R., Becker, M.,  
019 Benoit-Cattin, A., Bittig, H. C., Bopp, L., Bultan, S., Chandra, N., Chevallier, F., Chini, L. P., Evans, W., Florentie, L., Forster, P.  
020 M., Gasser, T., Gehlen, M., Gilfillan, D., Gkritzalis, T., Gregor, L., Gruber, N., Harris, I., Hartung, K., Haverd, V., Houghton, R. A.,  
021 Ilyina, T., Jain, A. K., Joetzjer, E., Kadono, K., Kato, E., Kitidis, V., Korsbakken, J. I., Landschützer, P., Lefèvre, N., Lenton, A.,

22 Lienert, S., Liu, Z., Lombardozi, D., Marland, G., Metz, N., Munro, D. R., Nabel, J. E. M. S., Nakaoka, S.-I., Niwa, Y., O'Brien,  
23 K., Ono, T., Palmer, P. I., Pierrot, D., Poulter, B., Resplandy, L., Robertson, E., Rödenbeck, C., Schwinger, J., Séférian, R., Skjelvan,  
24 I., Smith, A. J. P., Sutton, A. J., Tanhua, T., Tans, P. P., Tian, H., Tilbrook, B., van der Werf, G., Vuichard, N., Walker, A. P.,  
25 Wanninkhof, R., Watson, A. J., Willis, D., Wiltshire, A. J., Yuan, W., Yue, X., and Zaehe, S.: Global carbon budget 2020, *Earth*  
26 *Syst. Sci. Data*, 12, 3269–3340, 2020.

27 Friedlingstein, P., O'Sullivan, M., Jones, M. W., Andrew, R. M., Gregor, L., Hauck, J., Le Quéré, C., Lujikx, I. T., Olsen, A., Peters, G. P.,  
28 Peters, W., Pongratz, J., Schwingshackl, C., Sitch, S., Canadell, J. G., Ciais, P., Jackson, R. B., Alin, S. R., Alkama, R., Arneeth, A.,  
29 Arora, V. K., Bates, N. R., Becker, M., Bellouin, N., Bittig, H. C., Bopp, L., Chevallier, F., Chini, L. P., Cronin, M., Evans, W., Falk,  
30 S., Feely, R. A., Gasser, T., Gehlen, M., Gkritzalis, T., Gloege, L., Grassi, G., Gruber, N., Gürses, Ö., Harris, I., Hefner, M.,  
31 Houghton, R. A., Hurtt, G. C., Iida, Y., Ilyina, T., Jain, A. K., Jersild, A., Kadono, K., Kato, E., Kennedy, D., Klein Goldewijk, K.,  
32 Knauer, J., Korsbakken, J. I., Landschützer, P., Lefèvre, N., Lindsay, K., Liu, J., Liu, Z., Marland, G., Mayot, N., McGrath, M. J.,  
33 Metz, N., Monacci, N. M., Munro, D. R., Nakaoka, S.-I., Niwa, Y., O'Brien, K., Ono, T., Palmer, P. I., Pan, N., Pierrot, D., Pocock,  
34 K., Poulter, B., Resplandy, L., Robertson, E., Rödenbeck, C., Rodriguez, C., Rosan, T. M., Schwinger, J., Séférian, R., Shutler, J. D.,  
35 Skjelvan, I., Steinhoff, T., Sun, Q., Sutton, A. J., Sweeney, C., Takao, S., Tanhua, T., Tans, P. P., Tian, X., Tian, H., Tilbrook, B.,  
36 Tsujino, H., Tubiello, F., van der Werf, G. R., Walker, A. P., Wanninkhof, R., Whitehead, C., Willstrand Wranne, A., et al.: Global  
37 Carbon Budget 2022, *Earth System Science Data*, 14, 4811–4900, 2022.

38 Gatti, L. V., Basso, L. S., Miller, J. B., Gloor, M., Gatti Domingues, L., Cassol, H. L. G., Tejada, G., Aragão, L. E. O. C., Nobre, C.,  
39 Peters, W., Marani, L., Arai, E., Sanches, A. H., Corrêa, S. M., Anderson, L., Von Randow, C., Correia, C. S. C., Crispim, S. P., and  
40 Neves, R. A. L.: Amazonia as a carbon source linked to deforestation and climate change, *Nature*, 595, 388–393, 2021.

41 Gatti, L. V., Cunha, C. L., Marani, L., Cassol, H. L. G., Messias, C. G., Arai, E., Denning, A. S., Soler, L. S., Almeida, C., Setzer, A.,  
42 Domingues, L. G., Basso, L. S., Miller, J. B., Gloor, M., Correia, C. S. C., Tejada, G., Neves, R. A. L., Rajao, R., Nunes, F., Filho, B.,  
43 S. S., Schmitt, J., Nobre, C., Corrêa, S. M., Sanches, A. H., Aragão, L. E. O. C., Anderson, L., Von Randow, C., Crispim, S. P.,  
44 Silva, F. M., and Machado, G. B. M.: Increased Amazon carbon emissions mainly from decline in law enforcement, *Nature*, 621,  
45 318–323, 2023.

46 Grassi, G., Stehfest, E., Rogelj, J., van Vuuren, D., Cescatti, A., House, J., Nabuurs, G.-J., Rossi, S., Alkama, R., Viñas, R. A., Calvin, K.,  
47 Ceccherini, G., Federici, S., Fujimori, S., Gusti, M., Hasegawa, T., Havlik, P., Humpenöder, F., Korosuo, A., Perugini, L., Tubiello,  
48 F. N., and Popp, A.: Critical adjustment of land mitigation pathways for assessing countries' climate progress, *Nat. Clim. Chang.*, 11,  
49 425–434, 2021.

50 Grassi, G., Schwingshackl, C., Gasser, T., Houghton, R. A., Sitch, S., Canadell, J. G., Cescatti, A., Ciais, P., Federici, S., Friedlingstein, P.,  
51 Kurz, W. A., Sanz Sanchez, M. J., Abad Viñas, R., Alkama, R., Bultan, S., Ceccherini, G., Falk, S., Kato, E., Kennedy, D., Knauer,  
52 J., Korosuo, A., Melo, J., McGrath, M. J., Nabel, J. E. M. S., Poulter, B., Romanovskaya, A. A., Rossi, S., Tian, H., Walker, A. P.,  
53 Yuan, W., Yue, X., and Pongratz, J.: Harmonising the land-use flux estimates of global models and national inventories for 2000–  
54 2020, *Earth System Science Data*, 15, 1093–1114, 2023.

55 Hartmann, J., Jansen, N., Dürr, H. H., Kempe, S., and Köhler, P.: Global CO<sub>2</sub>-consumption by chemical weathering: What is the  
56 contribution of highly active weathering regions?, *Glob. Planet. Change*, 69, 185–194, 2009.

57 Höglund-Isaksson, L., Gómez-Sanabria, A., Klimont, Z., Rafaj, P., and Schöpp, W.: Technical potentials and costs for reducing global  
58 anthropogenic methane emissions in the 2050 timeframe –results from the GAINS model, *Environ. Res. Commun.*, 2, 025004, 2020.

59 IPCC: Revised 1996 IPCC Guidelines for National Greenhouse Inventories, IPCC/OECD/IEA, Paris, France, 1997.

60 IPCC: 2006 IPCC guidelines for National Greenhouse Gas Inventories, IGES, 2006.

61 IPCC: 2019 Refinement to the 2006 IPCC Guidelines for National Greenhouse Gas Inventories, edited by: Buendia, E., Tanabe, K.,  
62 Kranjc, A., Baasansuren, J., Fukuda, M., Ngarize, S., Osako, A., Pyrozhenko, Y., Shermanau, P., and Federici, S., Intergovernmental  
63 Panel on Climate Change (IPCC), Switzerland, 2019.

64 IPCC: Climate Change 2023: Synthesis Report, IPCC, Geneva, Switzerland, 2023.

65 Janardanan, R., Maksyutov, S., Wang, F., Nayagam, L., Sahu, S., Mangaraj, P., Saunio, M., Lan, X., and Matsunaga, T.: Country-level  
66 methane emissions and their sectoral trends during 2009-2020 estimated by high-resolution inversion of GOSAT and surface  
67 observations, *Environmental Research Letters*, 19, 10.1088/1748-9326/ad2436, 2024

68 Janssens-Maenhout, G., Crippa, M., Guizzardi, D., Muntean, M., Schaaf, E., Dentener, F., Bergamaschi, P., Pagliari, V., Olivier, J. G. J.,  
69 Peters, J. A. H. W., van Aardenne, J. A., Monni, S., Doering, U., Petrescu, A. M. R., Solazzo, E., and Oreggioni, G. D.: EDGAR  
70 v4.3.2 Global Atlas of the three major greenhouse gas emissions for the period 1970–2012, *Earth Syst. Sci. Data*, 11, 959–1002,  
71 2019.

72 Jin, Z., Wang, T., Zhang, H., Wang, Y., Ding, J., and Tian, X.: Constraint of satellite CO<sub>2</sub> retrieval on the global carbon cycle from a  
73 Chinese atmospheric inversion system, *Sci. China Earth Sci.*, 66, 609–618, 2023.

74 Jones, M. W., Andrew, R. M., Peters, G. P., Janssens-Maenhout, G., De-Gol, A. J., Dou, X., Liu, Z., Pickers, P., Ciais, P., Patra, P. K.,  
75 Chevallier, F., and Le Quéré, C.: Gridded fossil CO<sub>2</sub> emissions and related O<sub>2</sub> combustion consistent with national inventories,  
76 2022.

77 Kaminski, T., Rayner, P. J., Heimann, M., and Enting, I. G.: On aggregation errors in atmospheric transport inversions, *J. Geophys. Res.*

78 D: Atmos., 106, 4703–4715, 2001.

79 Klein Goldewijk, K., Beusen, A., Doelman, J., and Stehfest, E.: Anthropogenic land use estimates for the Holocene – HYDE 3.2, Earth  
80 Syst. Sci. Data, 9, 927–953, 2017.

81 Kong, Y., Zheng, B., Zhang, Q., and He, K.: Global and regional carbon budget for 2015–2020 inferred from OCO-2 based on an  
82 ensemble Kalman filter coupled with GEOS-Chem, Atmos. Chem. Phys., 22, 10769–10788, 2022.

83 van der Laan-Luijkx, I. T., van der Velde, I. R., van der Veen, E., Tsuruta, A., Stanislawska, K., Babenhauserheide, A., Zhang, H. F., Liu,  
84 Y., He, W., Chen, H., Masarie, K. A., Krol, M. C., and Peters, W.: The CarbonTracker Data Assimilation Shell (CTDAS) v1.0:  
85 implementation and global carbon balance 2001–2015, Geosci. Model Dev., 10, 2785–2800, 2017.

86 Lauvaux, T., Giron, C., Mazzolini, M., d’Apremont, A., Duren, R., Cusworth, D., Shindell, D., and Ciais, P.: Global assessment of oil and  
87 gas methane ultra-emitters, Science, 375, 557–561, 2022.

88 Liu, J., Baskaran, L., Bowman, K., Schimel, D., Bloom, A. A., Parazoo, N. C., Oda, T., Carroll, D., Menemenlis, D., Joiner, J., Commane,  
89 R., Daube, B., Gatti, L. V., McKain, K., Miller, J., Stephens, B. B., Sweeney, C., and Wofsy, S.: Carbon Monitoring System Flux  
90 Net Biosphere Exchange 2020 (CMS-Flux NBE 2020), Earth System Science Data, 13, 299–330, 2021.

91 Maksyutov, S., Oda, T., Saito, M., Janardanan, R., Belikov, D., Kaiser, J. W., Zhuravlev, R., Ganshin, A., Valsala, V. K., Andrews, A.,  
92 Chmura, L., Dlugokencky, E., Haszpra, L., Langenfelds, R. L., Machida, T., Nakazawa, T., Ramonet, M., Sweeney, C., and Worthy,  
93 D.: Technical note: A high-resolution inverse modelling technique for estimating surface CO<sub>2</sub> fluxes based on the NIES-TM–  
94 FLEXPART coupled transport model and its adjoint, Atmos. Chem. Phys., 21, 1245–1266, 2021.

95 Mason Earles, J., Yeh, S., and Skog, K. E.: Timing of carbon emissions from global forest clearance, Nat. Clim. Chang., 2, 682–685, 2012.

96 Mayorga, E., Seitzinger, S. P., Harrison, J. A., Dumont, E., Beusen, A. H. W., Bouwman, A. F., Fekete, B. M., Kroeze, C., and Van  
97 Drecht, G.: Global Nutrient Export from WaterSheds 2 (NEWS 2): Model development and implementation, Environmental  
98 Modelling & Software, 25, 837–853, 2010.

99 Naus, S., Domingues, L. G., Krol, M., Luijkx, I. T., Gatti, L. V., Miller, J. B., Gloor, E., Basu, S., Correia, C., Koren, G., Worden, H. M.,  
:00 Flemming, J., Pétron, G., and Peters, W.: Sixteen years of MOPITT satellite data strongly constrain Amazon CO fire emissions,  
:01 Atmos. Chem. Phys., 22, 14735–14750, 2022.

:02 Niwa, Y., Ishijima, K., Ito, A., and Iida, Y.: Toward a long-term atmospheric CO<sub>2</sub> inversion for elucidating natural carbon fluxes:  
:03 technical notes of NISMON-CO<sub>2</sub> v2021.1, Progress in Earth and Planetary Science, 9, 1–19, 2022.

:04 Ogle, S. M., Domke, G., Kurz, W. A., Rocha, M. T., Huffman, T., Swan, A., Smith, J. E., Woodall, C., and Krug, T.: Delineating managed  
:05 land for reporting national greenhouse gas emissions and removals to the United Nations framework convention on climate change,

06 Carbon Balance Manag., 13, 9, 2018.

07 Patra, P. K., Takigawa, M., Watanabe, S., Chandra, N., Ishijima, K., and Yamashita, Y.: Improved Chemical Tracer Simulation by  
08 MIROC4.0-based Atmospheric Chemistry-Transport Model (MIROC4-ACTM), SOLAIAT, 14, 91–96, 2018.

09 Patra, P. K., Dlugokencky, E. J., Elkins, J. W., Dutton, G. S., Tohjima, Y., Sasakawa, M., Ito, A., Weiss, R. F., Manizza, M., Krummel, P.  
10 B., Prinn, R. G., O’doherly, S., Bianchi, D., Nevison, C., Solazzo, E., Lee, H., Joo, S., Kort, E. A., Maity, S., and Takigawa, M.:  
11 Forward and Inverse Modelling of Atmospheric Nitrous Oxide Using MIROC4-Atmospheric Chemistry-Transport Model, Journal of  
12 the Meteorological Society of Japan. Ser. II, 100, 361–386, 2022.

13 Peng, S., Lin, X., Thompson, R. L., Xi, Y., Liu, G., Hauglustaine, D., Lan, X., Poulter, B., Ramonet, M., Saunio, M., Yin, Y., Zhang, Z.,  
14 Zheng, B., and Ciais, P.: Wetland emission and atmospheric sink changes explain methane growth in 2020, Nature, 612, 477–482,  
15 2022.

16 Perugini, L., Pellis, G., Grassi, G., Ciais, P., Dolman, H., House, J. I., Peters, G. P., Smith, P., Günther, D., and Peylin, P.: Emerging  
17 reporting and verification needs under the Paris Agreement: How can the research community effectively contribute?, Environ. Sci.  
18 Policy, 122, 116–126, 2021.

19 Petrescu, A. M. R., McGrath, M. J., Andrew, R. M., Peylin, P., Peters, G. P., Ciais, P., Broquet, G., Tubiello, F. N., Gerbig, C., Pongratz,  
20 J., Janssens-Maenhout, G., Grassi, G., Nabuurs, G.-J., Regnier, P., Lauerwald, R., Kuhnert, M., Balkovič, J., Schelhaas, M.-J., Denier  
21 van der Gon, H. A. C., Solazzo, E., Qiu, C., Pilli, R., Kononov, I. B., Houghton, R. A., Günther, D., Perugini, L., Crippa, M.,  
22 Ganzenmüller, R., Luijkx, I. T., Smith, P., Munassar, S., Thompson, R. L., Conchedda, G., Monteil, G., Scholze, M., Karstens, U.,  
23 Brockmann, P., and Dolman, A. J.: The consolidated European synthesis of CO2 emissions and removals for the European Union  
24 and United Kingdom: 1990–2018, Earth Syst. Sci. Data, 13, 2363–2406, 2021.

25 Philibert, A., Loyce, C., and Makowski, D.: Prediction of N2O emission from local information with Random Forest, Environ. Pollut.,  
26 177, 156–163, 2013.

27 Potapov, P., Hansen, M. C., Laestadius, L., Turubanova, S., Yaroshenko, A., Thies, C., Smith, W., Zhuravleva, I., Komarova, A.,  
28 Minnemeyer, S., and Esipova, E.: The last frontiers of wilderness: Tracking loss of intact forest landscapes from 2000 to 2013, Sci  
29 Adv, 3, e1600821, 2017.

30 Regnier, P., Friedlingstein, P., Ciais, P., Mackenzie, F. T., Gruber, N., Janssens, I. A., Laruelle, G. G., Lauerwald, R., Luysaert, S.,  
31 Andersson, A. J., Arndt, S., Arnosti, C., Borges, A. V., Dale, A. W., Gallego-Sala, A., Goddérís, Y., Goossens, N., Hartmann, J.,  
32 Heinze, C., Ilyina, T., Joos, F., LaRowe, D. E., Leifeld, J., Meysman, F. J. R., Munhoven, G., Raymond, P. A., Spahni, R.,  
33 Suntharalingam, P., and Thullner, M.: Anthropogenic perturbation of the carbon fluxes from land to ocean, Nat. Geosci., 6, 597–607,

2013.

Rödenbeck, C., Houweling, S., Gloor, M., and Heimann, M.: CO<sub>2</sub> flux history 1982–2001 inferred from atmospheric data using a global inversion of atmospheric transport, *Atmos. Chem. Phys.*, 3, 1919–1964, 2003.

Saunois, M., Stavert, A. R., Poulter, B., Bousquet, P., Canadell, J. G., Jackson, R. B., Raymond, P. A., Dlugokencky, E. J., Houweling, S., Patra, P. K., Ciais, P., Arora, V. K., Bastviken, D., Bergamaschi, P., Blake, D. R., Brailsford, G., Bruhwiler, L., Carlson, K. M., Carrol, M., Castaldi, S., Chandra, N., Crevoisier, C., Crill, P. M., Covey, K., Curry, C. L., Etiope, G., Frankenberg, C., Gedney, N., Hegglin, M. I., Höglund-Isaksson, L., Hugelius, G., Ishizawa, M., Ito, A., Janssens-Maenhout, G., Jensen, K. M., Joos, F., Kleinen, T., Krummel, P. B., Langenfelds, R. L., Laruelle, G. G., Liu, L., Machida, T., Maksyutov, S., McDonald, K. C., McNorton, J., Miller, P. A., Melton, J. R., Morino, I., Müller, J., Murguía-Flores, F., Naik, V., Niwa, Y., Noce, S., O'Doherty, S., Parker, R. J., Peng, C., Peng, S., Peters, G. P., Prigent, C., Prinn, R., Ramonet, M., Regnier, P., Riley, W. J., Rosentretter, J. A., Segers, A., Simpson, I. J., Shi, H., Smith, S. J., Steele, L. P., Thornton, B. F., Tian, H., Tohjima, Y., Tubiello, F. N., Tsuruta, A., Viovy, N., Voulgarakis, A., Weber, T. S., van Weele, M., van der Werf, G. R., Weiss, R. F., Worthy, D., Wunch, D., Yin, Y., Yoshida, Y., Zhang, W., Zhang, Z., Zhao, Y., Zheng, B., Zhu, Q., Zhu, Q., and Zhuang, Q.: The global methane budget 2000–2017, *Earth Syst. Sci. Data*, 12, 1561–1623, 2020.

Saunois, M., Martínez, A., Poulter, B., Zhang, Z., Raymond, P., Regnier, P., Canadell, J. G., Jackson, R. B., Patra, P. K., Bousquet, P., Ciais, P., Dlugokencky, E. J., Lan, X., Allen, G. H., Bastviken, D., Beerling, D. J., Belikov, D. A., Blake, D. R., Castaldi, S., Crippa, M., Deemer, B. R., Dennison, F., Etiope, G., Gedney, N., Höglund-Isaksson, L., Holgerson, M. A., Hopcroft, P. O., Hugelius, G., Ito, A., Jain, A. K., Janardanan, R., Johnson, M. S., Kleinen, T., Krummel, P., Lauerwald, R., Li, T., Liu, X., McDonald, K. C., Melton, J. R., Mühle, J., Müller, J., Murguía-Flores, F., Niwa, Y., Noce, S., Pan, S., Parker, R. J., Peng, C., Ramonet, M., Riley, W. J., Rocher-Ros, G., Rosentretter, J. A., Sasakawa, M., Segers, A., Smith, S. J., Stanley, E. H., Thanwerdas, J., Tian, H., Tsuruta, A., Tubiello, F. N., Weber, T. S., van der Werf, G., Worthy, D. E., Xi, Y., Yoshida, Y., Zhang, W., Zheng, B., Zhu, Q., Zhu, Q., and Zhuang, Q.: Global Methane Budget 2000–2020, *Earth Syst. Sci. Data Discuss.* [preprint], <https://doi.org/10.5194/essd-2024-115>, in review, 2024.

Schuld, K. N., Mund, J., Lujikx, I. T., Aalto, T., Abshire, J. B., Aikin, K., Andrews, A., Aoki, S., Apadula, F., Baier, B., Bakwin, P., Bartyzel, J., Bentz, G., Bergamaschi, P., Beyersdorf, A., Biermann, T., Biraud, S. C., Boenisch, H., Bowling, D., Brailsford, G., van den Bulk, P., Chen, G., Chen, H., Chmura, L., Clark, S., Climadat, S., Della Coletta, J., Colomb, A., Commene, R., Conil, S., Cox, A., Cristofanelli, P., Cuevas, E., Curcoll, R., Daube, B., Davis, K., Delmotte, M., DiGangi, J. P., van Dinter, D., Dlugokencky, E., Elkins, J. W., Emmenegger, L., Fang, S., Fischer, M. L., Forster, G., Frumau, A., Galkowski, M., Gatti, L. V., Gehrlein, T., Gerbig,



.62 C., Gheusi, F., Gloor, E., Gomez-Trueba, V., Goto, D., Griffis, T., Hammer, S., Hanson, C., Haszpra, L., Hatakka, J., Heimann, M.,  
.63 Heliasz, M., Hensen, A., Hermanssen, O., Hints, E., Holst, J., Ivakhov, V., Jaffe, D., Joubert, W., Karion, A., Kawa, S. R., Kazan,  
.64 V., Keeling, R., Keronen, P., Kolari, P., Kominkova, K., Kort, E., Kozlova, E., Krummel, P., Kubistin, D., Labuschagne, C., Lam, D.  
.65 H. Y., Langenfelds, R., Laurent, O., Laurila, T., Lauvaux, T., Lavric, J., Law, B., Lee, J., Lee, O. S. M., Lehner, I., Leppert, R.,  
.66 Leuenberger, M., Levin, I., Levula, J., Lin, J., Lindauer, M., Loh, Z., Lopez, M., Machida, T., et al.: Multi-laboratory compilation of  
.67 atmospheric carbon dioxide data for the period 1957-2020; obspack\_co2\_1\_GLOBALVIEWplus\_v7.0\_2021-08-18, 2021.  
.68 Schuldt, K. N., Jacobson, A. R., Aalto, T., Andrews, A., Bakwin, P., Bergamaschi, P., Biermann, T., Biraud, S. C., Chen, H., Colomb, A.,  
.69 Conil, S., Cristofanelli, P., Delmotte, M., Dlugokencky, E., Emmenegger, L., Fischer, M. L., Hatakka, J., Heliasz, M., Hermanssen,  
.70 O., Holst, J., Jaffe, D., Karion, A., Kazan, V., Keronen, P., Kominkova, K., Kubistin, D., Laurent, O., Laurila, T., Lee, J., Lehner, I.,  
.71 Leuenberger, M., Lindauer, M., Lopez, M., Mammarella, I., Manca, G., Marek, M. V., De Mazière, M., McKain, K., Miller, C. E.,  
.72 Miller, J. B., Mölder, M., Müller-Williams, J., Myhre, C. L., Piacentino, S., Pichon, J. M., Plass-Duelmer, C., Plass-Duelmer, C.,  
.73 Ramonet, M., di Sarra, A. G., Scheeren, B., Schumacher, M., Sha, M. K., Sloop, C. D., Smith, P., Steinbacher, M., Sweeney, C.,  
.74 Tans, P., Thoning, K., Tørseth, K., Trisolino, P., Viner, B., Vitkova, G., and De Wekker, S.: Multi-laboratory compilation of  
.75 atmospheric carbon dioxide data for the year 2022; obspack\_co2\_1\_NRT\_v7.2\_2022-06-28, 2022.  
.76 Segers, A. and Houweling, S.: Description of the CH4 Inversion Production Chain, Copernicus Atmosphere Monitoring Service, 2017.  
.77 Shcherbak, I., Millar, N., and Robertson, G. P.: Global metaanalysis of the nonlinear response of soil nitrous oxide (N<sub>2</sub>O) emissions to  
.78 fertilizer nitrogen, Proc. Natl. Acad. Sci. U. S. A., 111, 9199–9204, 2014.  
.79 Thompson, R. L., Chevallier, F., Crotwell, A. M., Dutton, G., Langenfelds, R. L., Prinn, R. G., Weiss, R. F., Tohjima, Y., Nakazawa, T.,  
.80 Krummel, P. B., Steele, L. P., Fraser, P., O'Doherty, S., Ishijima, K., and Aoki, S.: Nitrous oxide emissions 1999 to 2009 from a  
.81 global atmospheric inversion, Atmos. Chem. Phys., 14, 1801–1817, 2014.  
.82 Tian, H., Yang, J., Xu, R., Lu, C., Canadell, J. G., Davidson, E. A., Jackson, R. B., Arneth, A., Chang, J., Ciais, P., Gerber, S., Ito, A.,  
.83 Joos, F., Lienert, S., Messina, P., Olin, S., Pan, S., Peng, C., Saikawa, E., Thompson, R. L., Vuichard, N., Winiwarter, W., Zaehle, S.,  
.84 and Zhang, B.: Global soil nitrous oxide emissions since the preindustrial era estimated by an ensemble of terrestrial biosphere  
.85 models: Magnitude, attribution, and uncertainty, Glob. Chang. Biol., 25, 640–659, 2019.  
.86 Tian, H., Xu, R., Canadell, J. G., Thompson, R. L., Winiwarter, W., Suntharalingam, P., Davidson, E. A., Ciais, P., Jackson, R. B.,  
.87 Janssens-Maenhout, G., Prather, M. J., Regnier, P., Pan, N., Pan, S., Peters, G. P., Shi, H., Tubiello, F. N., Zaehle, S., Zhou, F.,  
.88 Arneth, A., Battaglia, G., Berthet, S., Bopp, L., Bouwman, A. F., Buitenhuis, E. T., Chang, J., Chipperfield, M. P., Dangal, S. R. S.,  
.89 Dlugokencky, E., Elkins, J. W., Eyre, B. D., Fu, B., Hall, B., Ito, A., Joos, F., Krummel, P. B., Landolfi, A., Laruelle, G. G.,

.90 Lauerwald, R., Li, W., Lienert, S., Maavara, T., MacLeod, M., Millet, D. B., Olin, S., Patra, P. K., Prinn, R. G., Raymond, P. A.,  
.91 Ruiz, D. J., van der Werf, G. R., Vuichard, N., Wang, J., Weiss, R. F., Wells, K. C., Wilson, C., Yang, J., and Yao, Y.: A  
.92 comprehensive quantification of global nitrous oxide sources and sinks, *Nature*, 586, 248–256, 2020.

.93 Tian, H., Pan, N., Thompson, R. L., Canadell, J. G., Suntharalingam, P., Regnier, P., Davidson, E. A., Prather, M., Ciais, P., Muntean, M.,  
.94 Pan, S., Winiwarter, W., Zaehle, S., Zhou, F., Jackson, R. B., Bange, H. W., Berthet, S., Bian, Z., Bianchi, D., Bouwman, A. F.,  
.95 Buitenhuis, E. T., Dutton, G., Hu, M., Ito, A., Jain, A. K., Jeltsch-Thömmes, A., Joos, F., Kou-Giesbrecht, S., Krummel, P. B., Lan,  
.96 X., Landolfi, A., Lauerwald, R., Li, Y., Lu, C., Maavara, T., Manizza, M., Millet, D. B., Mühle, J., Patra, P. K., Peters, G. P., Qin, X.,  
.97 Raymond, P., Resplandy, L., Rosentreter, J. A., Shi, H., Sun, Q., Tonina, D., Tubiello, F. N., van der Werf, G. R., Vuichard, N.,  
.98 Wang, J., Wells, K. C., Western, L. M., Wilson, C., Yang, J., Yao, Y., You, Y., and Zhu, Q.: Global Nitrous Oxide Budget 1980–  
.99 2020, *Earth System Science Data Discussions*, 1–98, 2023.

.00 Tibrewal, K., Ciais, P., Saunois, M., Martinez, A., Lin, X., Thanwerdas, J., Deng, Z., Chevallier, F., Giron, C., Albergel, C., Tanaka, K.,  
.01 Patra, P., Tsuruta, A., Zheng, B., Belikov, D., Niwa, Y., Janardanan, R., Maksyutov, S., Segers, A., Tzompa-Sosa, Z. A., Bousquet,  
.02 P., and Sciare, J.: Assessment of methane emissions from oil, gas and coal sectors across inventories and atmospheric inversions,  
.03 *Commun. Earth Environ.*, 5, <https://doi.org/10.1038/s43247-023-01190-w>, 2024.

.04 Tsuruta, A., Aalto, T., Backman, L., Hakkarainen, J., van der Laan-Luijkx, I. T., Krol, M. C., Spahni, R., Houweling, S., Laine, M.,  
.05 Dlugokencky, E., Gomez-Pelaez, A. J., van der Schoot, M., Langenfelds, R., Ellul, R., Arduini, J., Apadula, F., Gerbig, C., Feist, D.  
.06 G., Kivi, R., Yoshida, Y., and Peters, W.: Global methane emission estimates for 2000–2012 from CarbonTracker Europe-CH4 v1.0,  
.07 *Geosci. Model Dev.*, 10, 1261–1289, 2017.

.08 UNFCCC: Biennial Update Report submissions from Non-Annex I Parties, available at: <https://unfccc.int/BURs>, last access: 2 July 2021a.

.09 UNFCCC: National Communication submissions from Non-Annex I Parties, available at: <https://unfccc.int/non-annex-I-NCs>, last access:  
.10 5 December 2021b.

.11 Wang, J. A., Baccini, A., Farina, M., Randerson, J. T., and Friedl, M. A.: Disturbance suppresses the aboveground carbon sink in North  
.12 American boreal forests, *Nat. Clim. Chang.*, 11, 435–441, 2021.

.13 Wang, Q., Zhou, F., Shang, Z., Ciais, P., Winiwarter, W., Jackson, R. B., Tubiello, F. N., Janssens-Maenhout, G., Tian, H., Cui, X.,  
.14 Canadell, J. G., Piao, S., and Tao, S.: Data-driven estimates of global nitrous oxide emissions from croplands, *Natl Sci Rev*, 7, 441–  
.15 452, 2020.

.16 van Wees, D., van der Werf, G. R., Randerson, J. T., Rogers, B. M., Chen, Y., Veraverbeke, S., Giglio, L., and Morton, D. C.: Global  
.17 biomass burning fuel consumption and emissions at 500 m spatial resolution based on the Global Fire Emissions Database (GFED),

18 Geoscientific Model Development, 15, 8411–8437, 2022.

19 Wells, K. C., Millet, D. B., Bousserez, N., Henze, D. K., Chaliyakunnel, S., Griffis, T. J., Luan, Y., Dlugokencky, E. J., Prinn, R. G.,  
20 O’Doherty, S., Weiss, R. F., Dutton, G. S., Elkins, J. W., Krummel, P. B., Langenfelds, R., Steele, L. P., Kort, E. A., Wofsy, S. C.,  
21 and Umezawa, T.: Simulation of atmospheric N<sub>2</sub>O with GEOS-Chem and its adjoint: evaluation of observational constraints, *Geosci.*  
22 *Model Dev.*, 8, 3179–3198, 2015.

23 Wilson, C., Chipperfield, M. P., Gloor, M., and Chevallier, F.: Development of a variational flux inversion system (INVICAT v1.0) using  
24 the TOMCAT chemical transport model, *Geosci. Model Dev.*, 7, 2485–2500, 2014.

25 Winkler, K., Yang, H., Ganzenmüller, R., Fuchs, R., Ceccherini, G., Duveiller, G., Grassi, G., Pongratz, J., Bastos, A., Shvidenko, A.,  
26 Araza, A., Herold, M., Wigneron, J.-P., and Ciais, P.: Changes in land use and management led to a decline in Eastern Europe’s  
27 terrestrial carbon sink, *Communications Earth & Environment*, 4, 1–14, 2023.

28 Xu, X., Sharma, P., Shu, S., Lin, T.-S., Ciais, P., Tubiello, F. N., Smith, P., Campbell, N., and Jain, A. K.: Global Greenhouse Gas  
29 Emissions from Plant-and Animal-Based Food, *Nature Food*, 2021.

30 Yao, Y., Tian, H., Shi, H., Pan, S., Xu, R., Pan, N., and Canadell, J. G.: Increased global nitrous oxide emissions from streams and rivers  
31 in the Anthropocene, *Nat. Clim. Chang.*, 10, 138–142, 2019.

32 Yin, Y., Chevallier, F., Ciais, P., Broquet, G., Fortems-Cheiney, A., Pison, I., and Saunois, M.: Decadal trends in global CO emissions as  
33 seen by MOPITT, *Atmos. Chem. Phys.*, 15, 13433–13451, 2015.

34 Zheng, B., Chevallier, F., Ciais, P., Yin, Y., Deeter, M. N., Worden, H. M., Wang, Y., Zhang, Q., and He, K.: Rapid decline in carbon  
35 monoxide emissions and export from East Asia between years 2005 and 2016, *Environ. Res. Lett.*, 13, 044007, 2018.

36 Zhou, F., Shang, Z., Zeng, Z., Piao, S., Ciais, P., Raymond, P. A., Wang, X., Wang, R., Chen, M., Yang, C., Tao, S., Zhao, Y., Meng, Q.,  
37 Gao, S., and Mao, Q.: New model for capturing the variations of fertilizer-induced emission factors of N<sub>2</sub>O, *Global Biogeochem.*  
38 *Cycles*, 29, 885–897, 2015.

39 Zscheischler, J., Mahecha, M. D., Avitabile, V., Calle, L., Carvalhais, N., Ciais, P., Gans, F., Gruber, N., Hartmann, J., Herold, M., Ichii,  
40 K., Jung, M., Landschützer, P., Laruelle, G. G., Lauerwald, R., Papale, D., Peylin, P., Poulter, B., Ray, D., Regnier, P., Rödenbeck,  
41 C., Roman-Cuesta, R. M., Schwalm, C., Tramontana, G., Tyukavina, A., Valentini, R., van der Werf, G., West, T. O., Wolf, J. E.,  
42 and Reichstein, M.: Reviews and syntheses: An empirical spatiotemporal description of the global surface–atmosphere carbon fluxes:  
43 opportunities and data limitations, *Biogeosciences*, 14, 3685–3703, 2017.

44

45

